



HAL
open science

Initial deformation of the northern Tibetan plateau: insights from deposition of the Lulehe Formation in the Qaidam Basin

Feng Cheng, Carmala Garziona, Marc Jolivet, Zhaojie Guo, Daowei Zhang,
Changhao Zhang, Qiquan Zhang

► To cite this version:

Feng Cheng, Carmala Garziona, Marc Jolivet, Zhaojie Guo, Daowei Zhang, et al.. Initial deformation of the northern Tibetan plateau: insights from deposition of the Lulehe Formation in the Qaidam Basin. *Tectonics*, 2019, 38 (2), pp.741-766. 10.1029/2018TC005214 . insu-01999656

HAL Id: insu-01999656

<https://insu.hal.science/insu-01999656>

Submitted on 13 Mar 2019

HAL is a multi-disciplinary open access archive for the deposit and dissemination of scientific research documents, whether they are published or not. The documents may come from teaching and research institutions in France or abroad, or from public or private research centers.

L'archive ouverte pluridisciplinaire **HAL**, est destinée au dépôt et à la diffusion de documents scientifiques de niveau recherche, publiés ou non, émanant des établissements d'enseignement et de recherche français ou étrangers, des laboratoires publics ou privés.

Tectonics

RESEARCH ARTICLE

10.1029/2018TC005214

Key Points:

- We carry out flexural modeling to estimate the initial topographic load of the Qilian Shan and Eastern Kunlun Shan
- Lulehe Formation consists of distal fluvial-marginal lacustrine and proximal fluvial-alluvial fan deposits along the margins of the basin
- Both Qilian Shan and Eastern Kunlun Shan topographic loads account for the initial subsidence of the Qaidam basin

Supporting Information:

- Supporting Information S1

Correspondence to:

F. Cheng,
cfcf.chengfeng@gmail.com;
fcheng5@ur.rochester.edu

Citation:

Cheng, F., Garzzone, C. N., Jolivet, M., Guo, Z., Zhang, D., Zhang, C., & Zhang, Q. (2019). Initial deformation of the northern Tibetan Plateau: Insights from deposition of the Lulehe Formation in the Qaidam Basin. *Tectonics*, 38. <https://doi.org/10.1029/2018TC005214>

Received 2 JUL 2018

Accepted 23 JAN 2019

Accepted article online 29 JAN 2019

Initial Deformation of the Northern Tibetan Plateau: Insights From Deposition of the Lulehe Formation in the Qaidam Basin

Feng Cheng^{1,2} , Carmala N. Garzzone¹, Marc Jolivet³, Zhaojie Guo⁴ , Daowei Zhang⁵, Changhao Zhang⁵, and Qiquan Zhang⁵

¹Department of Earth and Environmental Sciences, University of Rochester, Rochester, NY, USA, ²State Key Laboratory of Loess and Quaternary Geology, Institute of Earth Environment, CAS, Xi'an, China, ³Laboratoire Géosciences Rennes, CNRS-UMR6118, Université Rennes 1, Observatoire des Sciences de l'Univers, Rennes, France, ⁴Key Laboratory of Orogenic Belts and Crustal Evolution, Ministry of Education, School of Earth and Space Sciences, Peking University, Beijing, China, ⁵Qinghai Oilfield Company, PetroChina, Dunhuang, Gansu, China

Abstract The Paleogene Lulehe Formation marks the onset of deposition in the Qaidam basin and preserves evidence of the initial topographic growth of northern Tibet. However, limited outcrops impede understanding of the sedimentary features of the Lulehe Formation as well as the tectonic relationship between the basin and surrounding topography. To fill this gap, we investigated core samples along the basin margin and conducted flexural modeling to estimate the topographic load of the Qilian Shan and Eastern Kunlun Shan during the deposition of the Lulehe Formation. Core samples reveal that the Lulehe Formation mainly consists of distal fluvial to marginal lacustrine deposits and proximal fluvial deposits along the southern margin of the basin while characterized by proximal alluvial fan deposits along the northern margin of the basin. Together with evidence for faulting shown on the seismic profiles, we infer that simultaneous deformation within the Qilian Shan and Altyn Tagh Shan during the Paleogene resulted in accumulation of coarse detrital deposits in the northwestern and northeastern Qaidam basin. The simultaneous deformation within the Altyn Tagh Shan and Qilian Shan since the Paleogene supports the idea that deformation in these two regions is kinematically linked. One- and two-load beam flexural modeling indicates that the topographic load generated by both the Eastern Kunlun Shan and the Qilian Shan is responsible for the subsidence of the Qaidam basin during deposition of the Lulehe Formation. Our results highlight the initial relative high topography in the northern Tibetan plateau during the early Cenozoic.

1. Introduction

Continued collision between India and Asia since circa 60–45 Ma has driven the growth and crustal deformation of the Tibetan plateau (e.g., Dupont-Nivet et al., 2010; Garzanti and Van Haver, 1988; Green et al., 2008; Hu et al., 2015; W. Huang et al., 2015; Hu et al., 2016; Najman et al., 2010; Rowley, 1996). However, the kinematics and dynamics of the Tibetan plateau remain highly debated (Bird, 1991; Clark, 2012; Clark et al., 2010; Dewey & Bird, 1970; Duvall et al., 2011; England & Houseman, 1986; Molnar & Tapponnier, 1975; Royden et al., 1997; Tapponnier et al., 2001; Van Hinsbergen et al., 2012; C. Wang et al., 2008; W. Wang, Zheng, et al., 2017; Yin, Dang, Wang, et al., 2008; Yin, Dang, Zhang, et al., 2008; Yin & Harrison, 2000). The Qaidam basin, situated in the northern Tibetan plateau (Figure 1a), is filled with up to ~14 km of Cenozoic clastic sedimentary rocks that preserve a complete record of the intraplate response to the India-Asia collision (Bush et al., 2016; Cheng, Fu, et al., 2016; Cheng, Guo, et al., 2015; Cheng, Jolivet, et al., 2015; Cheng, Jolivet, et al., 2016; Molnar & Tapponnier, 1975; Meng & Fang, 2008; Meyer et al., 1998; Xia et al., 2001; Yin et al., 2007; Yin, Dang, Wang, et al., 2008; Yin, Dang, Zhang, et al., 2008; Zuza et al., 2016). This internally drained basin is bounded to the northwest by the lithospheric-scale left-lateral strike-slip Altyn Tagh Fault (ATF) that has accommodated hundreds of kilometers of crustal deformation in the northern Tibetan plateau (Figure 1a; Cheng, Guo, et al., 2015; Cheng, Jolivet, et al., 2016; Gehrels et al., 2003; Ritts & Biffi, 2000; Yin, Dang, Zhang, et al., 2008; Yin et al., 2002; Yue & Liou, 1999). Despite recent vast improvements in the sedimentation and deformation history database for the Qaidam basin (Bush et al., 2016; Cheng, Fu, et al., 2016; Cheng, Guo, et al., 2015; Cheng, Jolivet, et al., 2015; Cheng, Jolivet,

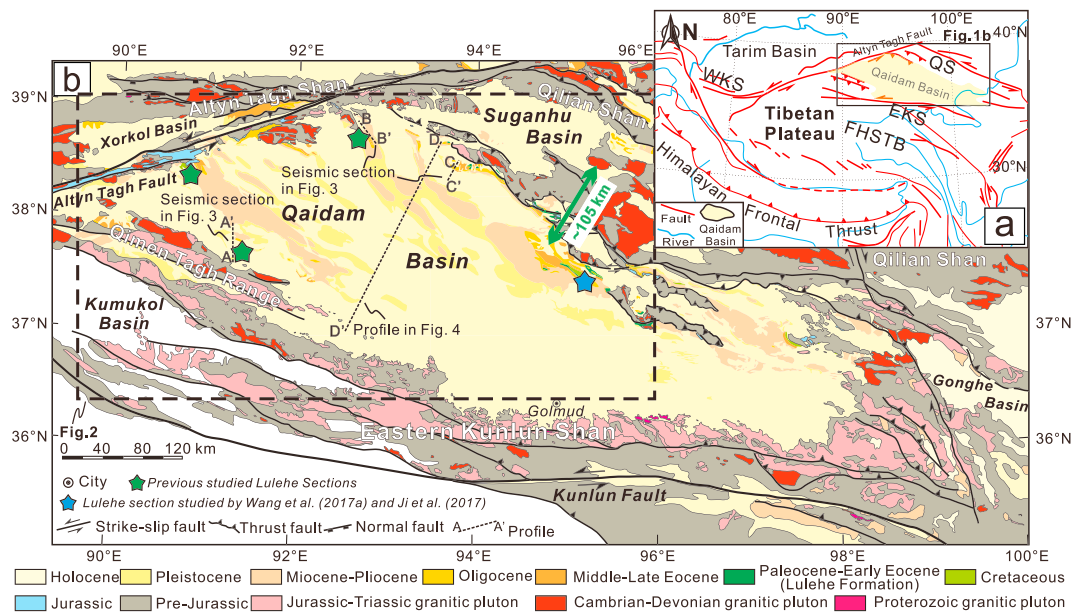


Figure 1. Geological map of research area and NE-SW oriented seismic profile beneath the Qaidam basin. (a) Sketch map of the Tibetan plateau, showing the major faults. QS = Qilian Shan; WKS = Western Kunlun Shan; EKS = Eastern Kunlun Shan; FHSTB = Fenghuoshan Thrust Belt. (b) Geological map of the Qaidam basin and surrounding area. The green stars refer to the Lulehe Fm. sections studied previously (Bush et al., 2016; Cheng, Fu, et al., 2016; Cheng, Jolivet, et al., 2016). The blue star refers to the Paleogene Lulehe Fm. section studied by W. Wang, Zheng, et al. (2017) and Ji et al. (2017). The green double arrows refer to the average width (~105 km) of the present-day southern Qilian Shan.

et al., 2016; Cheng et al., 2017; Fang et al., 2007; Lu & Xiong, 2009; Mao et al., 2014; Meng & Fang, 2008; Wu et al., 2014; Xia et al., 2001; Yin, Dang, Wang, et al., 2008; Yin, Dang, Zhang, et al., 2008; Zhuang et al., 2011), the evolution of the Paleogene Qaidam basin, and especially its initial topography and that of the surrounding mountain belts, remains elusive.

There are two critical questions concerning this poorly constrained issue. (1) Was the Eastern Kunlun Shan already exhumed during the early Cenozoic, causing the separation of the Qaidam basin and the Hoh Xil basin? And (2) were the ATF system and Qilian Shan Thrust Belt (QSTB) kinematically linked during the Paleogene after the India-Asia collision?

Comparing the stratigraphic characteristics of the Cenozoic strata of the Qaidam basin with those of the Hoh Xil basin to the south, Yin, Dang, Zhang, et al. (2008) suggested that they represented a single depression during the Paleogene, bounded to the north by the Qilian Shan and to the south by the Fenghuo Shan Thrust Belt (Figure 1a). This hypothesis has motivated reevaluation of the tectonic evolution within the northern Tibetan plateau (e.g., J.-L. Chen et al., 2018; Cheng et al., 2014; Mao et al., 2014; Shi et al., 2009; Staisch et al., 2014; C. S. Wang et al., 2011). If correct, this inference demonstrates that there should have been no, or relatively little, paleo-topography in the Eastern Kunlun Shan during the Paleogene. Combined with previously reported evidence of early Cenozoic deformation in the Qilian Shan region, this would indicate out-of-sequence deformation in the northern Tibetan plateau (evolving from the Qilian Shan to the Eastern Kunlun Shan southward, rather than the progressive northward growth). Such out of sequence deformation might be attributed to preexisting heterogeneity in mechanical strength in Tibetan lithosphere at the onset of India-Asian collision (Yin, Dang, Zhang, et al., 2008). However, this idea has been challenged by recent studies that propose pre-Paleogene exhumation of the Eastern Kunlun Shan based on the source to sink relationship between the Eastern Kunlun Shan and the Qaidam basin as well as the Hoh Xil basin (Bush et al., 2016; Cheng, Fu, et al., 2016; Li et al., 2017).

The second question posed above addresses the kinematic link between the ATF and QSTB. Marking the northern boundary of the Tibetan plateau, the ATF accommodates a significant amount of convergence between India and Eurasia through left-slip faulting. Ascertaining whether Paleogene deformation along the ATF is coupled with crustal shortening in the Qilian Shan is important for understanding the

kinematics of intraplate deformation associated with India-Asia collision and the dynamics of the Tibetan plateau growth (e.g., Allen et al., 2017; Meyer et al., 1998; Yin et al., 2002). If the Paleogene deformation along the ATF is coupled with crustal shortening in the QSTB, we can infer that the large amounts of sinistral displacement along the ATF since the India-Asia collision were largely absorbed by shortening in the Qilian Shan region. Otherwise, such a large amount of deformation would need to be accommodated through continued left-lateral strike-slip displacement along the ATF and transferred to the region further to the east, beyond the Tibetan plateau. By identifying Oligocene slip along the ATF, some researchers argued that the ATF extended well beyond its current northeastern tip into the Alxa region and further asserted that the full length of the ATF had already been established prior to initial shortening in the Qilian Shan (Darby et al., 2005; Yue et al., 2001; Yue et al., 2005). In contrast, others proposed that the ATF and QSTB are kinematically linked since initial Cenozoic subsidence of the Qaidam basin (e.g., Meyer et al., 1998; Xiao et al., 2015; Yin & Harrison, 2000; Yin, Dang, Zhang, et al., 2008; Zuza et al., 2016). Moreover, as the topographic evolution of the northern Tibetan plateau is assumed to determine the temporal and spatial evolution of the entire plateau during the Cenozoic (Bush et al., 2016; Clark et al., 2010; Cheng et al., 2014; Cheng, Fu, et al., 2016; Duvall et al., 2013; Lease et al., 2012; Lease, 2014; Yin et al., 2007; C. Wang et al., 2008; Yin, Dang, Wang, et al., 2008, Yin, Dang, Zhang, et al., 2008; Yuan et al., 2013; Zhuang et al., 2011), it is of primary importance to document the initial topography and structural relationship between the Qaidam basin and the surrounding mountain belts.

Flexural modeling provides insight into how topographic loads have varied to define flexural basin geometry (e.g., DeCelles, 2011; DeCelles & Giles, 1996; Royden & Karner, 1984). One goal of this study is to test two competing models for the evolution of the northern Tibetan plateau. Specifically, what topographic load (single Qilian Shan load vs. double loads from both the Qilian Shan and Eastern Kunlun Shan) in the northern Tibetan plateau may have existed in the early Cenozoic to generate the Qaidam basin? We thus analyzed isopach data of the Paleogene Lulehe Formation (Fm.) to conduct a 2-D flexural modeling experiment to investigate how the geometry of the early Cenozoic Qaidam basin was affected by loads created by the Qilian Shan to the north and Eastern Kunlun Shan to the south. In addition, to answer the question of whether the ATF system and QSTB are kinematically linked during the Paleogene after the India-Asia collision, we integrated three newly acquired high-quality seismic profiles with drill core samples from the Qaidam basin to constrain the Cenozoic onset of deformation within the surrounding mountain belts and to better describe the sedimentary characteristics of the Paleogene Lulehe Fm. within the basin and the structural pattern along its margins.

2. Geological Setting

2.1. Qaidam Basin

As the largest petroliferous basin within the Tibetan plateau, the triangle-shaped Qaidam basin is bounded by the Eastern Kunlun Shan to the south, the Altyn Tagh Shan to the northwest, and the Qilian Shan to the northeast (Figure 1b). Geological survey and petroleum exploration in recent decades indicate that the Qaidam basin contains >16 km of Mesozoic-Cenozoic clastic sedimentary fill (Cheng, Fu, et al., 2016; Cheng et al., 2017; Mao et al., 2014; Meng & Fang, 2008; Xia et al., 2001; Y. Y. Wang, Nie, et al., 2010; Wu et al., 2014; Yin, Dang, Wang, et al., 2008, Yin, Dang, Zhang, et al., 2008). The Mesozoic deposits are mainly distributed along the Altyn Tagh Shan and the Qilian Shan (Figure 1b; Cheng et al., 2019; Ritts et al., 1999; Wu et al., 2011; Zuza et al., 2017), while the Cenozoic deposits occur across the entire basin (Yin, Dang, Wang, et al., 2008; Mao et al., 2014). Based on outcrop investigation and subsurface data (including seismic profiles, well logs, and drill cores), the Cenozoic strata within the Qaidam basin are mainly subdivided into eight lithostratigraphic units (e.g., Rieser et al., 2006; Xia et al., 2001; Yin, Dang, Zhang, et al., 2008). These units are, from oldest to youngest, (1) the Lulehe Fm., $E_1 + 2$; (2) the Lower Xiaganchaigou Fm., E_3^1 xg; (3) the Upper Xiaganchaigou Fm., E_3^2 xg; (4) the Shangganhaigou Fm., N_1 sg; (5) the Xiayoushashan Fm., N_2^1 xy; (6) the Shangyoushashan Fm., N_2^2 sy; (7) the Shizigou Fm., N_2^3 s; and (8) the Qigequan Fm. (Q_1 q; Qiu, 2002; Song & Wang, 1993; E. Wang et al., 2006; Yin, Dang, Zhang, et al., 2008). Paleogene growth strata have been observed in the northwestern and northeastern Qaidam basin, indicating early Cenozoic deformation in the Altyn Tagh Shan and Qilian Shan (Cheng, Guo, et al., 2015; Cheng, Jolivet, et al., 2015; Cheng, Jolivet, et al., 2016; Yin et al., 2002; this study). Seismic profile interpretation and outcrop geology reveal that Miocene growth strata are widely developed throughout the basin, which indicates the

widespread Miocene tectonic deformation within the basin and along the surrounding mountain belts (Cheng et al., 2014; Cheng, Guo, et al., 2015; Cheng, Fu, et al., 2016; Cheng, Jolivet, et al., 2016; Mao et al., 2014; Meng & Fang, 2008; L. Wang, Xiao, et al., 2010; Wei et al., 2016; Wu et al., 2014; Yin et al., 2007; Yin, Dang, Wang, et al., 2008; Yin, Dang, Zhang, et al., 2008; Zhou et al., 2006).

The Lulehe Fm. marks the initiation of the Cenozoic clastic sedimentation in the Qaidam basin. Except for a few scattered deposits distributed in the southern front of the Altyn Tagh Shan, the Lulehe Fm. mainly outcrops within the northern Qaidam basin (Figure 1b; Bush et al., 2016; Ji et al., 2017; Z. Sun et al., 2005; W. Wang, Zheng, et al., 2017; Zhuang et al., 2011). Field investigation shows that the deposits in the northern Qaidam basin are mainly composed of pebble-cobble conglomerates interbedded with medium- to coarse-grained sandstones corresponding to alluvial fan to fluvial depositional environment (Bush et al., 2016; Huo, 1990; Xia et al., 2001; Zhuang et al., 2011). However, the sedimentary characteristics of the Lulehe Fm. that is deeply buried under the basin needs further documentation (Figures 1b and 2). The Lulehe Fm. is generally considered to be Paleocene to early Eocene in age (~50 Ma) based on magnetostratigraphy study, spore and pollen assemblages, regional lithostratigraphic correlation, and seismic reflection interpretation (Ji et al., 2017; Ke et al., 2013; Rieser et al., 2005, 2006; Xia et al., 2001; X. Wang et al., 2007; Yang et al., 1992; Yin et al., 2007; Yin, Dang, Wang, et al., 2008; Yin, Dang, Zhang, et al., 2008; Zhang, 2006; Zhuang et al., 2011). However, a recent magnetostratigraphy study of the Lulehe Fm. near the type locality in the northern Qaidam basin assigns an Oligocene (ca. 30 Ma) depositional age (W. Wang, Zheng, et al., 2017). Because the chronology of Lulehe Fm. is important for evaluating the intraplate response to the India-Asia collision and postcollision convergence, this debate highlights the need for further effort to determine the depositional age of the Lulehe Fm. strata throughout the entire Qaidam basin. Detailed discussion related to this age issue is given in the section 5.2.

2.2. Eastern Kunlun Shan, Altyn Tagh Shan, and Qilian Shan

The E-W oriented Eastern Kunlun Shan, with an average elevation of ~4.5 km, forms the southern morphological boundary of the Qaidam basin. The exhumation history the Eastern Kunlun Shan is complex, with an estimated onset age varying from the late Mesozoic to Miocene (Bush et al., 2016; Clark et al., 2010; X. Chen et al., 2010; X. Chen et al., 2011; Cheng, Fu, et al., 2016; ; Duvall et al., 2013; Jolivet et al., 2001, 2003; Mock et al., 1999; F. Wang et al., 2004; F. Wang, Shi, et al., 2017; Yin et al., 2007, Yi et al., 2008; Yin, Dang, Wang, et al., 2008; Yuan et al., 2006). The basement rocks and sediment cover within the Eastern Kunlun Shan are cut by the left-lateral strike-slip Kunlun fault that extends from the eastern edge of the Tibetan plateau to the east and terminates to the west with a splay structure including the Qimen Tagh Range (Cheng et al., 2014; Cheng, Fu, et al., 2016; Fu & Awata, 2007; Jolivet et al., 2003; Kirby et al., 2007; Lin & Guo, 2008). Cenozoic inception of the Kunlun fault is estimated to be circa 30–15 Ma, and the assessed total sinistral strike-slip displacement on the fault is circa 100 ± 20 km (Duvall et al., 2013; Fu & Awata, 2007; Jolivet et al., 2003; Kidd & Molnar, 1988; Kirby et al., 2007; Van Der Woerd et al., 2002; Yuan et al., 2006).

The SWW-NEE striking Altyn Tagh Shan, with an average elevation of ~4 km, defines the northwestern boundary of the Qaidam basin (Figure 1). It has experienced a multistage tectonic and exhumation history, from Mesozoic-Early Cenozoic to the present (Z. L. Chen et al., 2001; Cheng, Guo, et al., 2015; Delville et al., 2001; Jolivet et al., 1999; Jolivet et al., 2001; Jolivet et al., 2003; Ritts & Biffi, 2000; Sobel et al., 2001; Tapponnier et al., 1986; Y. Wang et al., 2005; E. Wang et al., 2006; Wu et al., 2012; Yin et al., 2002; Yue & Liou, 1999; Zhang et al., 2012). Within the range, the over 1,600-km-long left-lateral strike-slip ATF links the western Kunlun Shan to the southwest to the Qilian Shan to the northeast (Figure 1a; Burchfiel et al., 1989; E. Wang, 1997; Xiao et al., 2015; Yin et al., 2002; Yin & Harrison, 2000; Yue & Liou, 1999). The proposed Cenozoic age of initiation of the ATF varies from early Eocene (e.g., Yin et al., 2002) to late Eocene-early Oligocene (e.g., Z. L. Chen et al., 2001; Meng et al., 2001; Ritts et al., 2004; W. Wang et al., 2016; Yue et al., 2001) and finally to Miocene (e.g., Wan et al., 2001; Wu et al., 2012), and estimates of the total amount of displacement vary anywhere from approximately over 500 km to less than 90 km (Y. Chen et al., 2002; Cheng, Guo, et al., 2015; Cheng, Jolivet, et al., 2016; Darby et al., 2005; Gehrels et al., 2003; Ritts & Biffi, 2000; E. Wang, 1997; Yin et al., 2002; Yin, Dang, Zhang, et al., 2008; Yue & Liou, 1999; Yue et al., 2005).

The NW-SE trending Qilian Shan, with an average elevation of 4 km, marks the northern boundary of the Qaidam basin and the northeastern edge of the Tibetan plateau (Figure 1). This area contains a series of NW-SE oriented mountain ranges, namely, the QSTB, consisting of folds, thrusts, and strike-slip faults

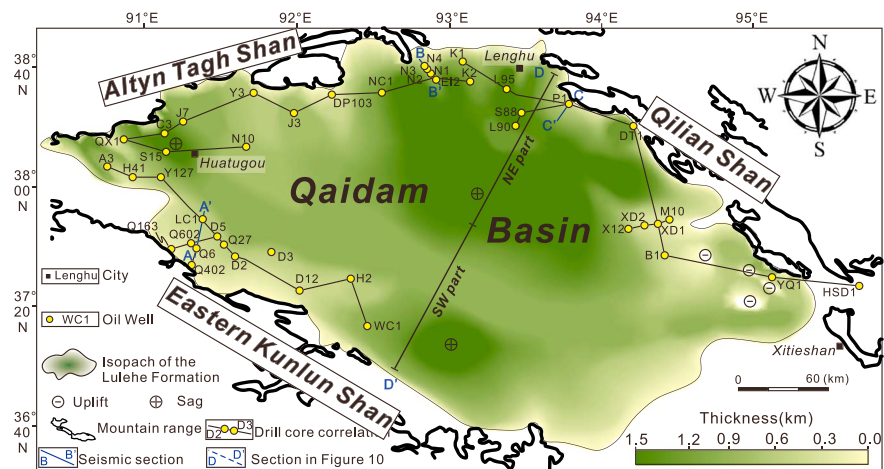


Figure 2. Isopach map of the Lulehe Formation and the distribution of the drilling wells used in this study. In recent years, Qinghai Oilfield, PetroChina, conducted petroleum exploration in the Qaidam basin and obtained abundant drill core and logging data from hundreds of the wells and abundant seismic data throughout the basin. Based on stratigraphic correlation, Lulehe Fm. isopach map was obtained and is widely acknowledged by geologists (e.g., Meng & Fang, 2008; Yin, Dang, Zhang, et al., 2008).

that accommodate considerable horizontal shortening and lateral motion of the crust (Bovet et al., 2009; Cheng, Jolivet, et al., 2015; Gaudemer et al., 1995; Meyer et al., 1998; Tapponnier et al., 2001; W. Wang et al., 2016; Yin & Harrison, 2000; Yin, Dang, Wang, et al., 2008; Zuza et al., 2016). Seismic profile interpretation, provenance analysis, and low-temperature thermochronometry, combined with field investigation, have revealed that crustal shortening and surface uplift began in the southern Qilian Shan and northern Qaidam basin during the Paleogene (W. Wang, Zheng, et al., 2017; Yin, Dang, Wang, et al., 2008; Zhuang et al., 2011; Zuza & Yin, 2016; Zuza et al., 2017). Deformation and uplift later propagated into the northern Qilian Shan and Hexi Corridor (Bovet et al., 2009; Lease, 2014; Meyer et al., 1998; W. Wang et al., 2016; Yin, Dang, Zhang, et al., 2008; Zheng et al., 2010; Zhuang et al., 2011).

3. Approach and Methods

3.1. Core Data and Seismic Profiles

To document the sedimentary characteristics of the Lulehe Fm., we present subsurface data provided by the Qinghai Oilfield, PetroChina, and a compilation of published stratigraphic data. Photos showing drill core samples are presented in Figure S1 in the supporting information. According to the petrological characteristics (e.g., grain size and mineralogy) and sedimentary structures (e.g., cross-bedding), lithofacies have been identified in drill cores from 48 wells mainly situated along the margins of the Qaidam basin (Figures 2). To show the distribution of the lithofacies of Lulehe Fm. in the Qaidam basin during the deposition of Lulehe Fm., six fence diagrams have been made (Figures S2–S7). In order to further decipher the Paleogene tectonic pattern, especially the onset of deformation, along the margin of the Qaidam basin, three high-quality seismic profiles acquired by the Qinghai Oilfield Company, PetroChina, have been provided. These three seismic reflection lines extend from the front of the surrounding mountain belts toward the center of the basin and intersect the boundary faults that root into the Eastern Kunlun Shan (section AA' in Figure 3), Altyn Tagh Shan (section BB' in Figure 3), and Qilian Shan (section CC' in Figure 3), respectively. The locations of these profiles are shown on Figures 1 and 2.

3.2. Flexural Loading Estimation

Previous studies have revealed that the geometry of a flexural basin is primarily related to the size and shape of the topographic load and to the parameters that govern the flexural behavior of the foreland lithosphere (e.g., Price, 1973). The width and depth of the flexural basin can be calculated, provided that the thickness and size of the topographic load, the density of the basin fill and topographic load, and the elastic properties of the flexural lithosphere are known (DeCelles, 2011; Jordan, 1981; Royden & Karner, 1984; Saylor et al.,

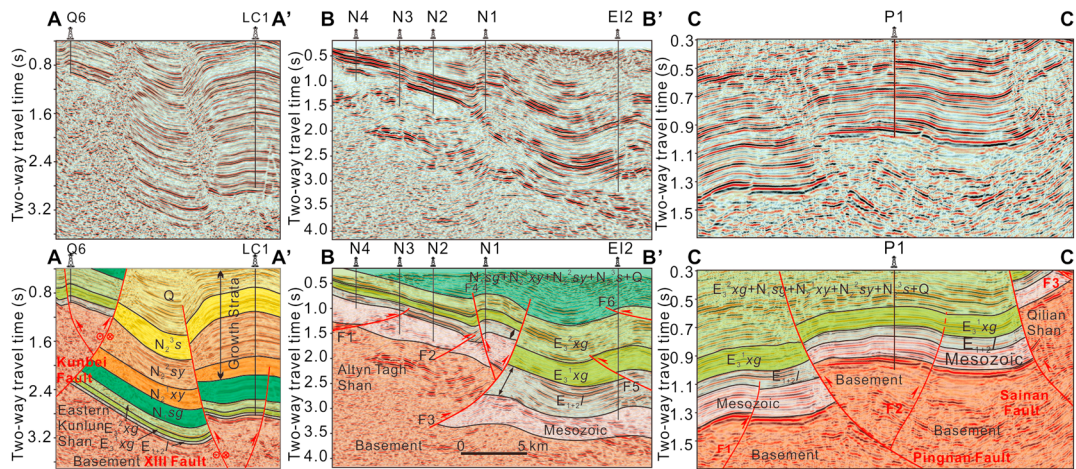


Figure 3. Original and interpreted seismic profiles. These three seismic reflection lines extend from the front of the surrounding mountain belt toward the center of the basin and intersect the boundary faults that root into the Eastern Kunlun Shan (section AA'), Alтын Tagh Shan (section BB'), and Qilian Shan (section CC'), respectively. Location of these profiles is shown in Figures 1 and 2. Q = Quaternary Qigequan Fm.; N_2^3s = Shizigou Fm.; N_2^2sy = Xiayoushashan Fm.; N_2^1xy = Xiayoushashan Fm.; N_1sg = Shangganchaigou Fm.; E_3^2xg = Upper Xiaganchaigou Fm.; E_3^1xg = Lower Xiaganchaigou Fm.; $E_1 + 2l$ = Lulehe Fm.

2017; Turcotte & Schubert, 2002; Wangen, 2010; Watts et al., 1980). The goal of this study is to understand whether a single Qilian Shan topographic load can produce the observed flexural profile of the Qaidam basin obtained by shortening restoration and decompaction in the earliest part of the basin history. To solve this problem, we define the Qaidam basin as a flexural basin and then conducted flexural modeling to estimate the required topographic load of the Qilian Shan and Eastern Kunlun Shan to account for the thickness and distribution of the Lulehe Fm.

In general, if the Eastern Kunlun Shan was not exhumed during the deposition of Lulehe Fm., we would expect that the Qaidam basin was a flexural basin and the deflection of the Qaidam basement was solely generated by the topography load of the Qilian Shan. On the other hand, if both the Eastern Kunlun Shan and the Qilian Shan were exhumed during the deposition of Lulehe Fm., the topographic load of both mountain ranges would contribute to the deflection of the Qaidam basement. In this study, we first calculated the original shape of the Qaidam basin during the deposition of Lulehe Fm. Given that the preexisting topography in the Qaidam basin would also affect the restoration estimates, we assume the Qaidam lithosphere was flat prior to the deposition of the Lulehe Fm. Existing 2-D and 3-D seismic profiles revealed minimal deformation within the Qaidam basin during the deposition of Lulehe Fm., especially in the interior of the basin (e.g., Cheng et al., 2014, Cheng, Fu, et al., 2016; Wei et al., 2016; Yin et al., 2007); we ignore the effects of deformation on the geometry of the basin. We then conducted one-load beam (only Qilian Shan load) and two-load beam (both Eastern Kunlun Shan and Qilian Shan loads) flexural modeling, respectively. Finally, we compared the original shape of the basin with the modeled deflection of the basin basement to address the question of whether a single Qilian Shan topographic load can produce the observed flexural shape of the Qaidam basin during the deposition of Lulehe Fm.

3.2.1. Original Shape of the Qaidam Basin

To obtain the original shape of the Qaidam basin during the deposition of Lulehe Fm., we selected a section DD' according to the isopach map of Lulehe Fm. strata (Figure 4). The isopach map of the Lulehe Fm. is provided by the Qinghai Oilfield Company, PetroChina. Over recent decades, Qinghai Oilfield, PetroChina, has conducted petroleum exploration in the Qaidam basin and obtained abundant drill core and logging data from hundreds of wells and abundant seismic data throughout the Qaidam basin. We note that the distribution of Lulehe Fm. is well-constrained along the margins, while the distribution of Lulehe Fm. in the central part of the basin is mainly stratigraphic correlation based on the seismic profiles.

Section DD' shows the present-day distribution of the Lulehe Fm. from the Qilian Shan to the Eastern Kunlun Shan. We then carried out shortening restoration and decompaction. Given that section DD' is approximately the same section provided by Wei et al. (2016), we followed the approach of Wei et al. (2016) and divided section DD' into two parts, namely, the southwest part and the northeast part,

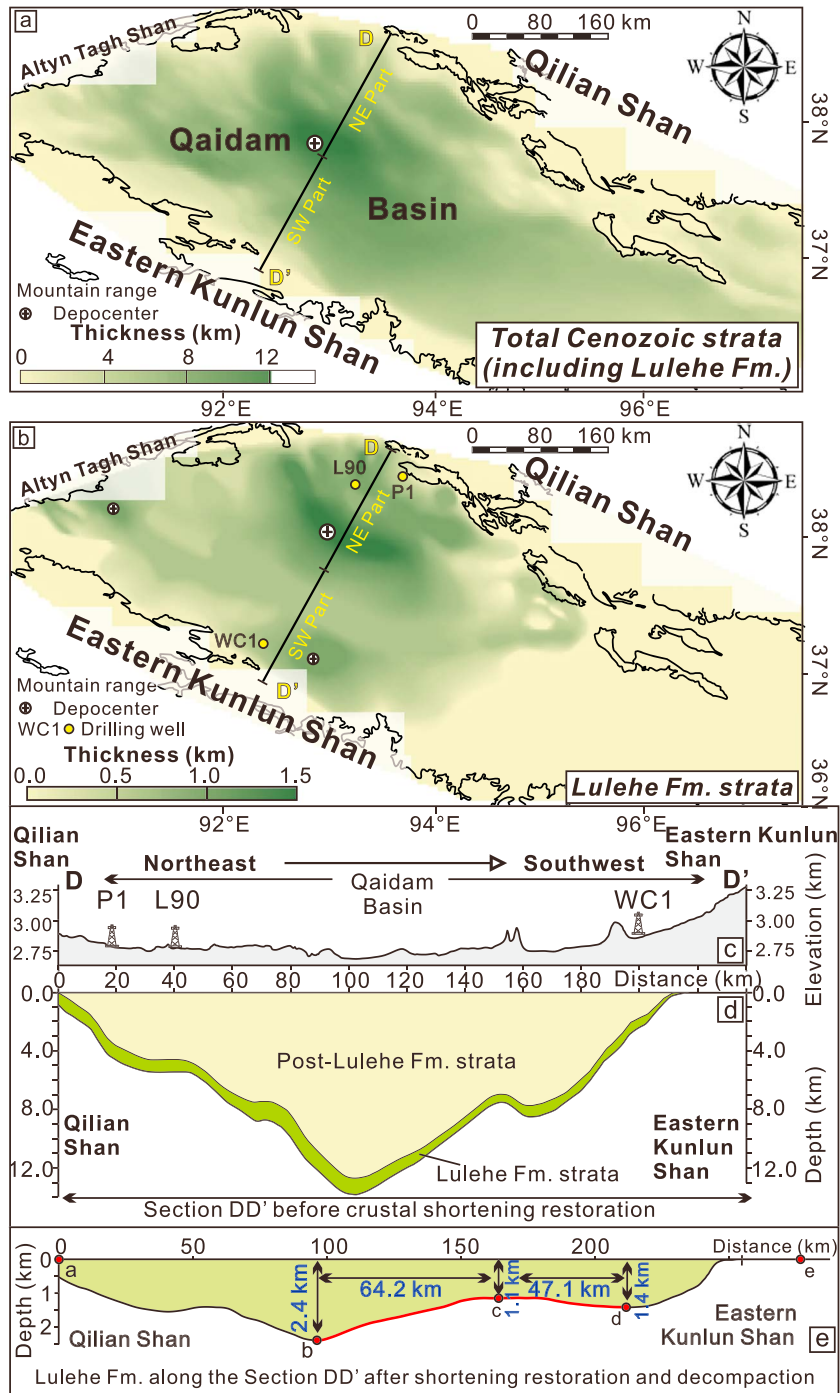


Figure 4. Distribution of the Cenozoic strata within the Qaidam basin. Isopach map of (a) the total Cenozoic stratigraphic thickness and (b) the Lulehe Fm. ($E_1 + 2l$). (c) NNE-SSW trending topographic profile DD' across the Qaidam basin. (d) Stratigraphic cross section across the Qaidam basin, showing the distribution of the Lulehe Fm. and post-Lulehe Fm. strata within the Qaidam basin. (e) Palinspastic section DD' after the shortening restoration and decompaction, showing the original shape of the Qaidam basin during the deposition of Lulehe Fm. Section DD' was divided into four segments, namely, a-b, b-c, c-d, and d-e.

respectively (Figures 4a and 4b). Based on 2-D regional seismic profiles, Yin, Dang, Zhang, et al. (2008) suggested a roughly 30% Cenozoic upper crustal shortening percent within the Qaidam basin. However, seismic reflection results provided by Wei et al. (2016) are more up-to-date, and the quality of those results have been significantly improved by the Qinghai Oilfield, PetroChina. We thus follow the estimated

shortening strain of Wei et al. (2016) and assumed that the southwest part of section DD' experienced 15% post-Lulehe shortening while the northeast part of section DD' experienced 13% post-Lulehe shortening. We thus restored the total length of section DD', which is perpendicular to the Qilian Shan, to determine the original width of the Qaidam basin. On the other hand, a palinspastically restored section DD' using the estimate of shortening strain (30%) of Yin, Dang, Zhang, et al. (2008) is shown in Figure S8 for comparison. The basin depth along section DD' was restored after conducting decompaction analysis. Given that the central basin is too deep to drill to the bottom, we are not able to obtain the lithologic information in the central part of the basin. The content of shale versus sandstone is calculated based on the lithologies encountered in wells WC1, L90, and P1 (Table 1). Considering the dominant alluvial fan-fluvial deposition in the Lulehe Fm., we assume the water depth is 0 m in this study. We then decompacted the Lulehe Fm. strata along section DD' across the basin, following the methods, porosity values, and porosity-depth coefficient of Sclater and Christie (1980). We thus obtain the original shape of section DD' during the deposition of the Lulehe Fm. (Figure 4e). In order to better compare the original shape of the basin obtained from shortening restoration and decompaction with flexural load modeling results, we further divided the original shape of the section DD' into four segments, namely, a-b, b-c, c-d, and d-e (Figure 4e). The terminology "wedge top" and "foredeep" can be generally applied to flexural basins that form adjacent to regions of crustal shortening and thickening regardless of whether the basin is formally defined as a foreland basin (Figure 5).

3.2.2. One-Load Beam Flexural Modeling

As shown on the isopach map, the Qaidam basin was not a symmetric basin during the deposition of Lulehe Fm., with its main depocenter close to the Qilian Shan (Figure 4b). Assuming that the single Qilian Shan topographic load accounts for the deflection of the Qaidam basement during the Lulehe Fm., segments a-b and b-c should correspond to "wedge top" and "foredeep," respectively. In addition, point b should correspond to the deepest of the basin (Figure 5b). We thus conducted one-load beam flexural modeling by assuming that the Eastern Kunlun Shan had not been deformed, and the Qilian Shan topographic load was solely responsible for the flexural subsidence of the Qaidam basin during the deposition of the Lulehe Fm. We estimated the flexural load estimate using the method of Turcotte and Schubert (2002) (localized load) as implemented in the Flexit programs (DeCelles, 2011) to obtain a modeled shape of the Qaidam basin (along the section DD') during the deposition of the Lulehe Fm. The input parameters are effective elastic thickness, mantle density, basin fill density, crustal density, and basin depth, which are listed in Table 1.

In the one-load beam model we assume that the single Qilian Shan topographic load accounts for the deflection of the Qaidam basement during the Lulehe Fm. To evaluate the subsidence of the Qaidam basin associated with flexural loading during the deposition of the Lulehe Fm. (Turcotte & Schubert, 2002), the Qaidam lithosphere was modeled as a broken (Figures 6a and 6b) and an infinite (Figures 6c and 6d) elastic plate, respectively, overlying a fluid asthenosphere ($\rho = 3,300 \text{ kg/m}^3$). The density of basin deposits varies between $1,550$ to $2,400 \text{ kg/m}^3$ and varies with depth (Allen & Allen, 2013). We take the basin load into consideration and assume the average density of basin fill is $2,000 \text{ kg/m}^3$. Given that the deepest part of a flexural basin corresponds to the edge of the topographic load, we thus apply the topographic load at point b (Figure 6) and define the depth of the basin to be 2.4 km. In order to show the variation in shape of the basin in response to effective elastic thickness, we calculated solutions for multiple values of effective elastic thickness (Figure 6).

3.2.3. Two-Load Beam Flexural Modeling

If the single Qilian Shan load is insufficient to account for the deflection of the Qaidam basement, then we assume that the Eastern Kunlun Shan was shortened and thickened, and both topographic loads account for the deflection of the Qaidam basin (Figure 5c). Segments a-b and b-c should correspond to the "wedge top" and "foredeep" of Qilian Shan load, respectively. Segments d-e and c-d should correspond to the "wedge top" and "foredeep" of Eastern Kunlun Shan load, respectively. Meanwhile, the Qilian Shan load would affect the deflection of parts c-d and d-e while the Eastern Kunlun Shan load would affect the deflection of parts a-b and b-c. Segment b-d along the section DD' represent the original shape of the Qaidam basin during the deposition of Lulehe Fm. We then conducted a two-load beam flexural modeling that assumes that both the Eastern Kunlun Shan and the Qilian Shan were deforming during the deposition of the Lulehe Fm. This two-load beam flexural model follows the method of Wangen (2010). We finally compared this two-

Table 1
Shortening Restoration, Decompaction, and Flexural Loading Estimates

Decompaction parameters									
Well Number	Content of shale (%)	Content of Sandstone (%)	Surface porosity of shale Φ_0 (%)	Surface porosity of sand Φ_0 (%)	Porosity-depth coefficient of shale C_{sh} (km^{-1})	Porosity-depth coefficient of sand C_{sa} (km^{-1})	Average Surface porosity Φ_{0a} (%)	Average Porosity-depth coefficient C_a (km^{-1})	Parts of the DD' transect (determine Φ_{0a} and C_a selection)
P1	51.3	48.7	0.63	0.49	0.51	0.27	0.56	0.39	D to P1
L90	95.34	4.7	0.63	0.49	0.51	0.27	0.62	0.50	P1 to WC1
WC1	69.7	30.3	0.63	0.49	0.51	0.27	0.59	0.44	WC1 to D'
Shortening restoration result									
Present-day length (km)					Shortening strain (%)	Restored length (km)	Horizontal distance between b and c (km)		Horizontal distance between b and d (km)
100					12.7	115	64		111
135					15.0	159			
235					13.9	273			
Decompaction result									
Depth of b (km)			Depth of c (km)			Depth of d (km)			Output Estimate result
2.4			1.1			1.4			
One load-beam flexural modeling (Flexit modeling)									
Input (Flexural loading parameters)									
Plate property	Mantle density (kg/m^3)	Basin fill density (kg/m^3)	Density contrast (kg/m^3)	Effective elastic thickness (km)	Flexural rigidity (Nm)	Depth of basin (km)	Flexural parameter (alpha) (km)	Basin width (km)	Forebulge height (m)
Broken	3.3×10^3	2.0×10^3	1.3×10^3	60	1.34×10^{24}	2.36	143.2	225.0	158.1
Broken	3.3×10^3	2.0×10^3	1.3×10^3	40	3.98×10^{23}	2.36	105.7	166.1	158.1
Broken	3.3×10^3	2.0×10^3	1.3×10^3	20	4.98×10^{22}	2.36	62.9	98.8	158.1
Broken	3.3×10^3	2.0×10^3	1.3×10^3	15	2.10×10^{22}	2.36	50.7	79.6	158.1
Broken	3.3×10^3	2.0×10^3	1.3×10^3	12	1.08×10^{22}	2.36	42.9	67.4	158.1
Broken	3.3×10^3	2.0×10^3	1.3×10^3	10	6.22×10^{21}	2.36	37.4	58.7	158.1
Infinite	3.3×10^3	2.0×10^3	1.3×10^3	60	1.34×10^{24}	2.36	143.2	337.5	102.0
Infinite	3.3×10^3	2.0×10^3	1.3×10^3	40	3.98×10^{23}	2.36	105.7	249.1	102.0
Infinite	3.3×10^3	2.0×10^3	1.3×10^3	20	4.98×10^{22}	2.36	62.9	148.2	102.0
Infinite	3.3×10^3	2.0×10^3	1.3×10^3	15	2.10×10^{22}	2.36	50.7	119.4	102.0
Infinite	3.3×10^3	2.0×10^3	1.3×10^3	10	6.22×10^{21}	2.36	37.4	88.1	102.0
Infinite	3.3×10^3	2.0×10^3	1.3×10^3	7	2.13×10^{21}	2.36	28.6	67.4	102.0
Infinite	3.3×10^3	2.0×10^3	1.3×10^3	6	1.34×10^{21}	2.36	25.5	60.0	102.0
Infinite	3.3×10^3	2.0×10^3	1.3×10^3	5	7.78×10^{20}	2.36	22.2	52.4	102.0

Table 1 (continued)

Two load-beam flexural modeling		Example 1		Example 2		Example 3		Example 4			
Gravity (m/s^2)	9.8	Mantle density (kg/m^3)	3.3×10^3	Basin fill density (kg/m^3)	2.0×10^3	Crust density (kg/m^3)	2.4×10^3	Effective elastic thickness (km)	30		
Topographic load		Best fit example		Example 1		Example 2		Example 3		Example 4	
		Qilian Shan	Eastern Kunlun Shan	Qilian Shan	Eastern Kunlun Shan	Qilian Shan	Eastern Kunlun Shan	Qilian Shan	Eastern Kunlun Shan	Qilian Shan	Eastern Kunlun Shan
Width (km)	150	180	180	100	180	150	230	150	130	150	130
Height (km)	2.5	1.2	1.2	3.0	1.2	2.5	0.8	2.5	1.7	2.5	1.7
Distance between center point of Qilian Shan and Eastern Kunlun Shan (km)	276		301		251		301		251		251

load-beam flexural modeling result with the original shape of the Qaidam basin to evaluate whether both loads are required to obtain the subsidence profile of the Qaidam basin.

To further evaluate the tectonic setting of the Qaidam basin, we run a two-load beam model by assuming that both the Eastern Kunlun Shan and the Qilian Shan deformation were responsible for the flexural subsidence of the Qaidam basin during deposition of the Lulehe Fm. Considering that the effective elastic thickness of the Qaidam lithosphere along the section DD' is around 30 km based on a synthesis of flexural parameter estimates over the Tibetan plateau (Braitenberg et al., 2003), we define the effective elastic thickness of the Qaidam lithosphere to be 30 km. To see how the effective elastic thickness of the Qaidam lithosphere would influence the deflection of the Qaidam basement, we also show two scenarios by defining the elastic thickness of the Qaidam lithosphere to be 20 and 40 km, respectively (Figure S9). In addition to the effective elastic thickness, four parameters further determine the modeled deflection of the Qaidam basement, namely, the height of Qilian Shan and Eastern Kunlun Shan, as well as the width of the Qilian Shan and Eastern Kunlun Shan. Previous studies have revealed that surface uplift began in the southern Qilian Shan and northern Qaidam basin during the Paleogene (W. Wang, Zheng, et al., 2017; Yin, Dang, Wang, et al., 2008; Zhuang et al., 2011; Zuza & Yin, 2016). Using Google Earth software, we measured the average width of the present-day southern Qilian Shan to be ~105 km (Figure 1b). Based on previous crustal shortening estimates in the Qilian Shan (Craddock et al., 2014; Gaudemer et al., 1995; Lease et al., 2012; Meyer et al., 1998; Wei et al., 2016; Yin, Dang, Wang, et al., 2008; Zuza et al., 2016; Zuza et al., 2017), we assigned a ~30% post-Lulehe Fm. crustal shortening in the southern Qilian Shan and thus assumed that the average width of the southern Qilian Shan during the deposition of Lulehe Fm. was ~150 km. As we do not know the height of the Qilian Shan and the Eastern Kunlun Shan, or the width of the Eastern Kunlun Shan, we thus tested different combinations of these parameters to determine a modeled deflection that can best fit the original shape of the Qaidam basin obtained from the shortening restoration and decompaction (segment b-d in section DD').

We point out that the Altyn Tagh Shan load to the northwest could have an influence on the deflection of the Qaidam basement. The present-day topographic distribution of the Altyn Tagh Shan is quite small compared with the distribution of the Eastern Kunlun Shan and Qilian Shan, although previous thermochronology studies suggest rapid exhumation of the basement rocks in the Altyn Tagh Shan during the Miocene (e.g., Jolivet et al., 1999, 2001). Given the limited distribution of the modern topographic load and the dominantly strike-slip displacement along the ATF, we consider the contribution of the Altyn Tagh Shan load to have been limited compared to the Eastern Kunlun Shan to the south and the Qilian Shan to the northeast during the deposition of Lulehe Fm.

We also note that the topographic profile of a mountain range is generally triangle shaped and using a distributed load may better describe the variation of the deflection in response to the load distribution. However, limited study of the timing and patterns of deformation of the Eastern Kunlun Shan and Qilian Shan during the deposition of the Lulehe Fm. precludes modeling the distributed load of the mountain ranges. We therefore choose a simplified approach in this study that assumes two rectangular loads to understand the general scale (i.e., relief and width) of the Eastern Kunlun Shan and Qilian Shan required to account for the shape of the deflection during the deposition of the Lulehe Fm. This simple model includes the following variables: the average height and width of Qilian Shan and Eastern Kunlun Shan loads, effective elastic thickness of Qaidam lithosphere, mantle density, basin fill density, crustal density, and the distance between the Eastern Kunlun Shan

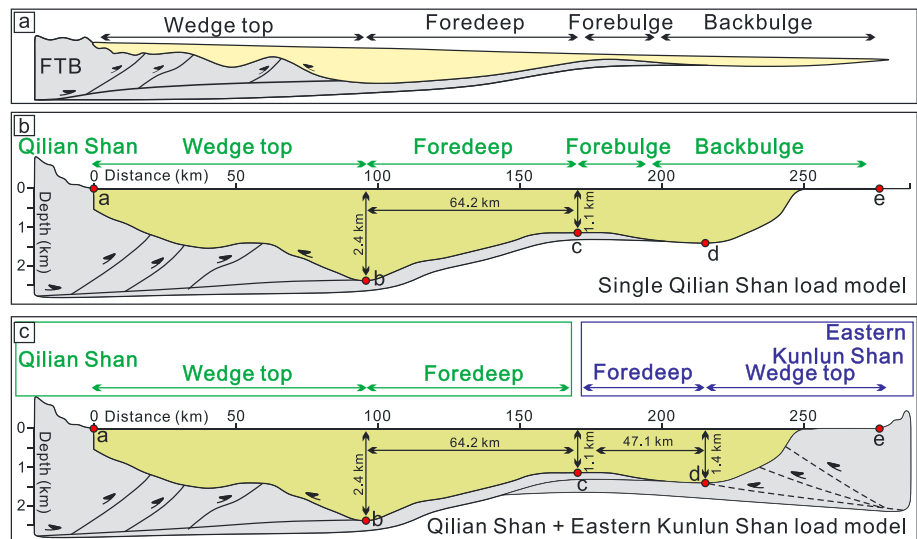


Figure 5. (a) Schematic cross section depicting a typical flexural basin system, with the wedge-top, foredeep, forebulge, and back-bulge depozones, modified from DeCelles and Giles (1996). (b) One-load beam model, assuming that the single Qilian Shan topographic load accounts for the deflection of the Qaidam basement. In this case, the segment a-b should correspond to the “wedge top,” and segment b-c correspond to the “foredeep.” (c) Two-load beam model, assuming that both the Qilian Shan and Eastern Kunlun Shan topographic loads are responsible for the subsidence of the Qaidam basin. In this case, segments a-b and b-c should correspond to the wedge top and foredeep of Qilian Shan load. Segments d-e and c-d should correspond to the wedge top and foredeep of Eastern Kunlun Shan load. The green area in (b) and (c) represents the original distribution of the Lulehe Fm. along the section DD’ after crustal shortening restoration and decompaction.

and the Qilian Shan. All of the parameters related to the flexural loading estimate, as well as the results, are listed in Table 1.

4. Results

4.1. Stratigraphy and Sedimentary Characteristics of the Lulehe Formation

Based on the 48 drill cores investigated in this study (Figures 2 and 3) and well-log data provided by the Qinghai Oilfield, PetroChina, three well correlations (fence diagrams) trending approximately parallel to the Eastern Kunlun Shan, Altyn Tagh Shan, and Qilian Shan, respectively, were established (Figures S2, S4, and S6). In addition, six well correlations (fence diagrams) running from the front of each mountain range to the center of the basin were built (Figures S3, S5, and S7).

4.1.1. SW Qaidam Basin (Northern Front of the Eastern Kunlun Shan)

Four drill cores from the westernmost part of the well correlation (wells S3, H41, Y127, and LC1) trending roughly parallel to the Eastern Kunlun Shan did not penetrate the entire Lulehe Fm. strata, and the observed successions in those wells are around 300–500 m thick (Figure S2). The lower part of the observed successions is mainly composed of reddish pebble-cobble conglomerate, fine-grained sandstone, and mudstone, while the middle and upper parts of the sequence are dominated by thick-bedded light brownish mudstone and sandy mudstone intercalated with mudstone and sandstone (Figure S2). In addition, the middle and upper parts of Lulehe Fm. in this region are marked by high natural gamma ray values indicative of a high shale content (Mu, 2002). Moreover, varve deposits and interbedded, thinly bedded marlstone are widely distributed (Mu, 2002; G. Sun, 2005). In the middle segment of the well correlation (wells D5, Q27, D2, D7, D5, and D12), drill cores generally penetrate the Lulehe Fm. strata and reach to the crystalline basement (Figures 3b and S2). The U-Pb zircon dating, whole-rock geochemistry, and Sr-Nd isotopic analyses of the core samples suggest that those basement rocks are mainly composed of Early Paleozoic and Late Paleozoic to Mesozoic granitic rocks that are fairly compatible with the coeval granitic rocks (similarities in the age and composition) found in the Eastern Kunlun Shan (Cheng et al., 2017). The Lulehe Fm. deposits observed in wells D5 and Q27 mainly consist of thickly bedded grayish and brownish mudstone, intercalated

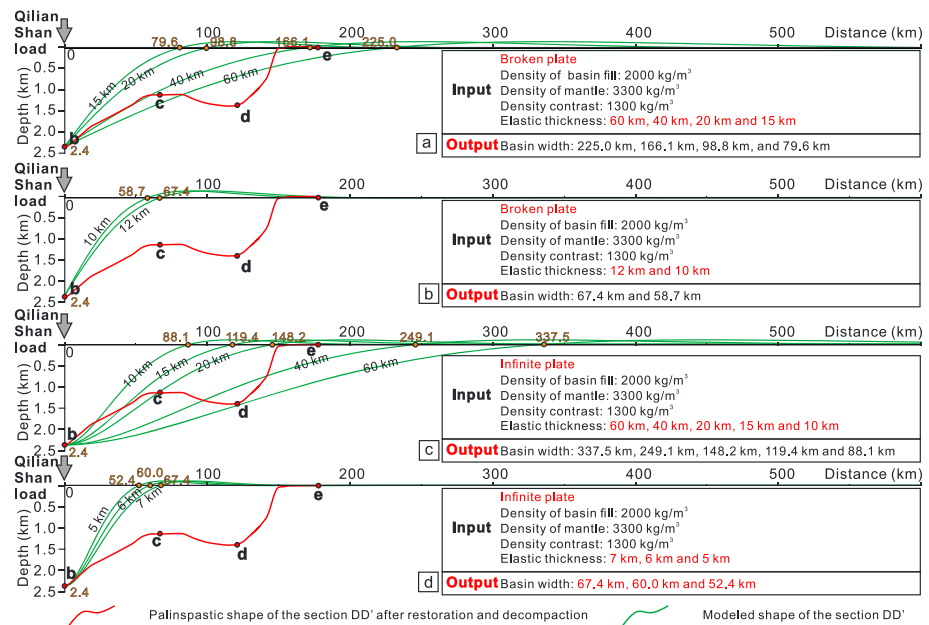


Figure 6. One-load beam flexural modeling results, assuming that the single Qilian Shan load accounted for the deflection of the Qaidam basement during the deposition of Lulehe Fm. (a) Flexural profile developed in response to a line load on a broken plate, with the effective elastic thickness of Qaidam lithosphere of 60, 40, 20, and 15 km, respectively. The modeled basin width is ~225.0, ~166.1, ~98.9, and ~79.6 km, respectively. (b) Flexural profile developed in response to a line load on a broken plate, with the effective elastic thickness of Qaidam lithosphere of 12 and 10 km, respectively. The modeled basin width is ~67.4 and ~58.7 km, respectively. (c) Flexural profile developed in response to a line load on an infinite plate, with the effective elastic thickness of Qaidam lithosphere of 60, 40, 20, 15, and 10 km, respectively. The modeled basin width is ~337.5, ~249.1, ~148.2, ~119.4, and ~88.1 km, respectively. (d) Flexural profile developed in response to a line load on an infinite plate, with effective elastic thickness of Qaidam lithosphere of 7, 6, and 5 km, respectively. The modeled basin width is ~67.4, ~60.0, and ~52.4 km, respectively. Note that the topographic load induced by the Qilian Shan alone fails to produce a sufficient deflection of the Qaidam basement during the deposition of the Lulehe Fm. regardless of the broken or infinite plate model and the effective elastic thickness assumed for the Qaidam lithosphere.

with thinly bedded sandstone (Figure S2). Carbonate-rich varves occurred in the middle and upper part of the cores (Ma & Wang, 2015).

To the east (wells D2, D7, D3, and D12), the lower and upper part of Lulehe Fm. is composed of a 10- to 100-m thickly reddish conglomerate and pebbly sandstone (Figures S1c, S1d, and S2). In this region, sandstones and conglomerates are structureless to cross-bedded and sometimes show scoured basal surfaces (Fu et al., 2012; Gong et al., 2012; Ma & Wang, 2015; Mo et al., 2013; Zhang et al., 2013). In contrast, the whole deposits above mainly consist of thickly bedded reddish-brownish carbonate-rich varved mudstone and fine-grained sandstone (Figures S1e, S1f, and S2; Ma & Wang, 2015). Further to the east, the drill cores again failed to reach the bottom of the Lulehe Fm. The observed succession (~400-m thick) is dominated by thick bedded fine-grain sandstone and sandy mudstone intercalated with thinly bedded sandstone (Figure S2; Fu et al., 2012; Gong et al., 2012; G. Sun, 2005; Zhang et al., 2013).

The two drill core correlations approximately perpendicular to the Eastern Kunlun Shan show that the Lulehe Fm. exhibits a thickness change toward the basin (Figure S3). As shown in wells Q163, Q602, Q402, and Q6, the lower part of the Lulehe Fm. deposited along the southern front of the Eastern Kunlun Shan is mainly composed of reddish pebble-cobble conglomerate while the middle and upper parts of the formation consist of mudstone, sandy mudstone, pebbly sandstone, and occasionally conglomerate (Figures S1g and S3; Fu et al., 2012; Gong et al., 2012; Zhang et al., 2013). Further toward the basin (wells D5 and LC1), the Lulehe Fm. is composed of thickly bedded grayish carbonate-rich varved mudstone (Figure S3; G. Sun, 2005).

We interpret that the Lulehe Fm. in the southwestern Qaidam basin is mainly characterized by proximal fluvial deposits with additional distal fluvial to marginal lacustrine deposits. Considering this gradual

lithofacies basinward transition (Figure S3), we infer a lake environment in the middle of the Qaidam basin during the deposition of Lulehe Fm. whereas the exact extent of the lake needs further investigation.

4.1.2. NW Qaidam Basin (Southern Front of the Altyn Tagh Shan)

Except for wells DP103 and EI2, the drill cores in the correlation profile parallel to the Altyn Tagh Shan failed to penetrate the entire Lulehe Fm. In the westernmost segment (well QX1), the observed Lulehe Fm. (600–1,000 m thick) is mainly composed of boulder to cobble sized conglomerate and pebbly sandstone intercalated with mudstone (Figure S4). In this region, these clasts are coarse grained, angular subrounded, poorly sorted, and clast supported with few mud matrix (G. Sun, 2005). In well C3, the sediments are mainly composed of reddish mudstone interbedded with reddish sandstone (Fu et al., 2012). Further east, in well J7 the sediments mainly consist of thick bedded grayish mudstone intercalated with thinly bedded sandstone and conglomerate, while the observed succession in the well J3 is composed of thickly bedded mudstone and marlstone interbedded with thinly bedded sandstone and conglomerate (Figure S4; G. Sun, 2005). In the central segment of the drill core correlation, the observed succession (>1,000 m thick) in well Y3 is dominated by thickly bedded pebbly sandstone and boulder to cobble sized conglomerate intercalated with thinly bedded mudstone (Figure S4; Fu et al., 2012). Clast-supported conglomerates are poorly sorted, and coarsening-upward cycles are present (Cao et al., 2013; G. Sun, 2005). In well DP103 (with ~800-m-thick deposits), the lower part of the observed succession is mainly composed of sandstone and sandy mudstone intercalated with boulder to cobble-sized conglomerate and pebbly sandstone (Figure S1h). Normally, graded bedding, cross-bedding, and scoured basal bedding surfaces are observed in this region (Figures 3h and S4; Cao et al., 2013; Fu et al., 2012; J. Huang et al., 2013). These deposits transition upward to thickly bedded mudstone intercalated with mudstone.

Further to the east, the observed succession (over 500 m thick) in well NC1 generally consists of thickly bedded varved mudstone intercalated with conglomerate, pebbly sandstone, and sandstone (Cao et al., 2013; Jiang et al., 2010). In the easternmost segment of the correlation (wells E12 and K2), the Lulehe Fm. (as thick as 1,500 m) is dominated by pebbly sandstone and clast-supported boulder to cobble-sized conglomerate intercalated with mudstone near the bottom (Figures 3i and S4; Cao et al., 2013; Fu et al., 2012; J. Huang et al., 2013). It transitions upward to thickly bedded grayish mudstone intercalated with sandstone (Figure S4; Cao et al., 2013; J. Huang et al., 2013).

In the two drill core correlations nearly perpendicular to the Altyn Tagh Shan (Figure S5), the Lulehe Fm. (wells QX1, N4, N3, N2, and N1) mainly consists of structureless coarse-grained, angular-subrounded, clast-supported conglomerate (Cao et al., 2013; J. Huang et al., 2013; Mu, 2002; G. Sun, 2005). Further basinward, the Lulehe Fm. (wells S15, N10, and E12) is marked by thickly bedded mudstone and sandy mudstone (Figure S1j; Cao et al., 2013; J. Huang et al., 2013; Mu, 2002; G. Sun, 2005).

Based on the core samples from several drill wells adjacent to Well DP103, J. Wang et al. (2013) also revealed that the Lulehe Fm. in this region mainly consists of boulder- to cobble-sized clast-supported conglomerates, indicative of a proximal alluvial fan deposits. The Lulehe Fm. in the northwestern Qaidam basin can thus be broadly characterized as dominated by boulder- to cobble-sized clast-supported conglomerate and pebbly sandstone, intercalated with mudstone and sandy mudstone, corresponding to the proximal alluvial fan deposits. The lack of matrix-supported boulder and cobble conglomerates points to a lack of debris flow deposition, instead reflecting fluvial-dominated alluvial fan deposition.

4.1.3. NE Qaidam Basin (Southern Front of the Qilian Shan)

Except for drill cores K1, DT1, B1, and YQ1, the cores in the transect parallel to the Qilian Shan penetrate the entire Lulehe Fm. and reach to the underlying Mesozoic strata or the granite basement (Figure S6; Cheng et al., 2017). In the western segment of the correlation (wells K1, L95, S88, P1, and DT1), the observed Lulehe Fm. is around 400 to 1,300 m thick (Figure S6; Fu et al., 2012). The lower part is dominated by boulder- to cobble-sized conglomerate and pebbly sandstone intercalated with sandy mudstone (Figure S6). These clasts are coarse grained, angular subrounded, poorly sorted, and clast supported with minor mud matrix, and normally, graded bedding, cross-bedding, and scoured surface are observed in this region (Figures S1k, S1l, and S6; Cao et al., 2013; J. Huang et al., 2013; Jiang et al., 2010; G. Sun et al., 2016). The upper part of the succession is mainly composed of mudstone intercalated with fine-grained sandstone and mudstone. Cross-bedding, bioturbation, and mud cracks occurred sporadically (Figure S6; Cao et al., 2013; Fu et al., 2012; Jiang et al., 2010; G. Sun et al., 2016). In the eastern segment (wells XD1, B1, YQ1, and HCD1), the Lulehe Fm. is only ~200 to 400 m thick and again mainly consists of boulder- to pebble-

sized conglomerate, pebbly sandstone intercalated with sandy mudstone. Conglomerates are clast supported. Coarse-grained, angular-subrounded, and poorly sorted clasts, cross-bedding, scoured surfaces are observed in this region (Figure S6; Fu et al., 2012; Jiang et al., 2010; H. Wang et al., 2014; Yang et al., 2013).

On the two drill core correlations approximately perpendicular to the Qilian Shan (Figure S7), the Lulehe Fm. along the southern flank of the Qilian Shan (wells P1, S88, XD1, and M10) mainly consists of structureless coarse-grained, angular-subrounded, and clast-supported conglomerate (Figure S11; Fu et al., 2012; Jiang et al., 2010; G. Sun et al., 2016; H. Wang et al., 2014; Yang et al., 2013). Further basinward, the Lulehe Fm. (wells L90 and X12) is marked by thickly bedded mudstone and sandy mudstone associated with a delta—lacustrine depositional environment (Fu et al., 2012).

Based on the core samples from several drill wells close to Well M10, Yang et al. (2013) also revealed that the Lulehe Fm. in this region mainly consist of boulder- to cobble-sized clast-supported conglomerates, indicative of a proximal alluvial fan deposits. In summary, based on the information we obtained from the observed drill core samples and previously published studies in this region, the Lulehe Fm. in the northeastern Qaidam basin is dominated by boulder- to pebble-sized clast-supported conglomerate and pebbly sandstone intercalated with mudstone and sandy mudstone, corresponding to the proximal alluvial fan deposits.

In general, the Lulehe Fm. deposited along the southern front of the Eastern Kunlun Shan (SW Qaidam basin) is mainly characterized by a mixture of proximal fluvial and distal fluvial to marginal lacustrine deposits (e.g. Fu et al., 2012; Gong et al., 2012; Ma & Wang, 2015; Mo et al., 2013; Mu, 2002; G. Sun, 2005; Zhang et al., 2013). On the other hand, along the southern flank of the Altyn Tagh Shan (NW Qaidam basin) and Qilian Shan (NE Qaidam basin), the Lulehe Fm. is characterized by proximal alluvial fan deposits (e.g., Cao et al., 2013; Fu et al., 2012; J. Huang et al., 2013; Jiang et al., 2010; Z. Sun et al., 2005; G. Sun et al., 2016; H. Wang et al., 2014; Yang et al., 2013). Dominant boulder- to pebble-sized conglomerate throughout the entire formation in both NW Qaidam basin and NE Qaidam basin indicates sedimentation by high-gradient depositional systems. Recent integrated research on the sedimentology, stratigraphy, and provenance of Qaidam basin fill has revealed that the basement of the Eastern Kunlun Shan, Altyn Tagh Shan, and Qilian Shan had already been exposed prior to the Paleogene, providing materials for the Qaidam basin (Cheng, Fu, et al., 2016; Cheng, Jolivet, et al., 2016; Yin, Dang, Zhang, et al., 2008; Zhuang et al., 2011; Zuza et al., 2016). Based on basinward lithofacies transitions, from proximal alluvial fan to fluvial deposits along the margins of the basin to distal fluvial to marginal lacustrine deposits basinward, as well as recent provenance analysis, we thus interpret that Qilian Shan, Altyn Tagh Shan, and Eastern Kunlun Shan had been exhumed by this time, serving as the sources of sediment to the Qaidam basin. In addition, the major topographic relief in the Eastern Kunlun Shan during deposition of Lulehe Fm. was located further south than its present-day location. Our analysis of sediment core samples generally displays gradual lithofacies basinward transitions, from proximal alluvial fan to fluvial deposits along the margins of the basin to distal fluvial to marginal lacustrine deposits basinward (Figures S3, S5, and S7).

4.2. Seismic Reflection Profile

4.2.1. Seismic Section AA'

The seismic section AA' runs from the northern front of the Eastern Kunlun Shan toward the central of western Qaidam basin, intersecting the Kunbei fault and the XIII fault (Figures 1 and 2). In this section, the Kunbei fault is a south-dipping high-angle thrust fault, rooted in the Eastern Kunlun Shan (Figure 3; Cheng et al., 2014). On both sides of the Kunbei fault, Mesozoic strata are lacking and Cenozoic deposits (including the Paleogene Lulehe Fm.) are identified. However, the thickness of the early Cenozoic deposits varies across the Kunbei fault showing obvious stratigraphic throw (Figure 3). Based on detailed isopach analyses and seismic profile interpretation, a previous study revealed that the sharp thickness variation of the Lulehe Fm. ($E_1 + 2l$), lower Xiaganchaigou Fm. ($E_3^1 \times g$), and upper Xiaganchaigou Fm. ($E_3^2 \times g$), from both sides of the Kunbei and XIII faults, resulted from lateral strike-slip movement on those faults during the Neogene (Cheng et al., 2014). Growth strata initiating in the hanging wall of the Kunbei and XIII faults during deposition of the Xiayoushashan Fm. ($N_2^1 \times y$) date the onset of deformation in the southwestern Qaidam basin (Figure 3). We thus propose that the faulting along the Kunbei and XIII faults might have accommodated uplift in the Eastern Kunlun Shan since the early Miocene (Clark et al., 2010; Duvall et al., 2013; Song & Wang, 1993; Yin et al., 2007; L. Wang, Xiao, et al., 2010) or since the middle Miocene using the chronology of W. Wang, Zheng, et al. [2017].

4.2.2. Seismic Section BB'

The seismic section BB' situated in the northwestern Qaidam basin, trends perpendicular to the Altyn Tagh Shan (Figures 1 and 2). On this section, several northwest dipping reverse faults (including faults F1, F2, and F3), rooting into the Altyn Tagh Shan, are identified (Figure 3). These basement-involved thrust faults offset the Mesozoic strata and die out in the Paleogene strata (Lulehe Fm.). In the hanging wall of fault F3 (that roots into the Altyn Tagh Shan) the Lulehe Fm. is characterized by relatively thin proximal alluvial fan deposits, while in the footwall of fault F3 they are represented by much thicker proximal alluvial fan deposits at the base, evolving upward to distal fluvial deposits (Figures 3 and S5). In addition, in the footwall of fault F3, generally northwestward-tapering growth strata within the Lulehe Fm. are developed, likely associated with Paleogene deformation within the Altyn Tagh Shan (Figure 3). We conclude that fault F3 initiated during the deposition of the Lulehe Fm., suggesting a Paleogene onset of deformation within the Altyn Tagh Shan.

4.2.3. Seismic Section CC'

Seismic section CC' is located in the northeastern Qaidam basin and trends from the southern Qilian Shan toward the central Qaidam basin (Figures 1 and 2). Two reverse faults (the Pingnan and Sainan faults), rooting into the Qilian Shan, are observed. The thickness of both the Mesozoic to early Cenozoic deposits varies across these faults showing obvious stratigraphic throw (Figure 3). The thickness changes in both the Mesozoic and early Cenozoic, as well as the southwestward-tapering growth strata within the Paleogene deposits, indicate deformation within the Qilian Shan in both the Mesozoic and the Paleogene (Figure 3), although the age gap between Mesozoic and Cenozoic deposits is uncertain. The F1 fault offsets the Mesozoic strata and dies out within the Paleogene strata (Lulehe Fm.), again suggesting that deformation in the northern Qaidam basin initiated in the Paleogene. This is consistent with the previous subsurface and outcrop constraints (Bush et al., 2016; Yin, Dang, Wang, et al., 2008; Yin, Dang, Zhang, et al., 2008; Zhuang et al., 2011).

From the data above, we conclude that the rapid uplift of the Eastern Kunlun Shan began in the early or middle Miocene (X. Chen et al., 2010; X. Chen et al., 2011), whereas the onset of tectonic deformation within both the Altyn Tagh Shan and the Qilian Shan began in the Paleogene, either ~50 Ma according to the previous chronological estimate (Ji et al., 2017; Ke et al., 2013; Rieser et al., 2005, 2006; Xia et al., 2001; Yang et al., 1992; Yin et al., 2007; Yin, Dang, Wang, et al., 2008; Yin, Dang, Zhang, et al., 2008; Zhang, 2006) or ~30 Ma using the chronology of W. Wang, Zheng, et al. [2017].

4.3. Flexural Loading Estimate

4.3.1. The Original Shape of the Basin After Shortening Restoration and Decompaction

Using the method described in the section 3.2, we obtained the original shape of section DD' (Figure 4e) during the deposition of Lulehe Fm. The horizontal length of the original section DD' is ~273 km. The horizontal length of segments b-c and c-d is ~64.2 and ~47.1 km, respectively. The depth of points b, c, and d is ~2.4, ~1.1, and ~1.4 km, respectively. See detailed results in Tables 1 and S1. As the water depth of the Qaidam basin during the deposition of the Lulehe Fm. is difficult to estimate, the obtained depth is considered the minimum depth.

4.3.2. Modeled Shape of the Basin Based on One-Load Beam Flexural Modeling

With regard to a broken plate model, the modeled basin width is ~225.0, ~166.1, ~98.8, and ~79.6 km when assigning a 60-, 40-, 20-, and 15-km effective elastic thickness to the Qaidam lithosphere, respectively (Figure 6a). The modeled basin width is much larger than the original shape of the basin after the shortening restoration and decompaction (represented by the horizontal width of segment b-c, 64.2 km). When assigning 12- and 10-km effective elastic thickness to the Qaidam lithosphere (Figure 6b), the modeled basin width is ~58.7 and ~67.4 km, respectively, which better fits the horizontal width of segment b-c (64.2 km).

For an infinite plate model, the modeled basin width is ~337.5, ~249.1, ~148.2, ~119.4, and ~88.1 km when assigning 60-, 40-, 20-, 15-, and 10-km effective elastic thickness to the Qaidam lithosphere, respectively (Figure 6c). The modeled basin shape is much wider than the original shape of the basin after shortening restoration and decompaction (represented by the horizontal width of segment b-c, 64.2 km). When assigning 7, 6, and 5 km to the Qaidam lithosphere (Figure 6d), the modeled basin width is ~67.4, ~60.0, and ~52.4 km, respectively, which better match with the horizontal length of segment b-c (64.2 km).

Our estimates show that the curvature of the calculated deflection is very sensitive to plate flexural rigidity (effective elastic thickness). An increase in the effective elastic thickness results in a decrease in the flexural curvature, which leads to a shallower and much wider basin. In contrast, the decrease in the effective elastic thickness tends to increase flexural curvature and localizes the deflection close to the topographically high part of the Qilian Shan (Figure 6). When assigning a relatively thin effective elastic thickness (12 to 5 km) to the Qaidam lithosphere, the modeled basin width can be better matched with the original width of the basin (Figures 6b and 6c). However, based on a synthesis of flexure parameters estimates over the Tibetan plateau by Braitenberg et al. (2003), the effective elastic thickness of the Qaidam lithosphere along the section DD' is not less than 30 km. Therefore, through the modeled basin width can be better matched with the original width of the basin, the assumption of a 5- to 12-km effective elastic thickness is problematic.

More importantly, the original shape of the Qaidam basin shows subsidence at the location of point d (1.4-km depth, horizontal width of segment b-d is 111.3 km). Our estimate reveals that one-load beam flexural modeling is not able to generate such a subsidence profile. We thus infer that the topographic load induced by the Qilian Shan alone fails to produce observed deflection of the Qaidam basement during the deposition of the Lulehe Fm. regardless of the broken or infinite plate model, the effective elastic thickness assumed for the Qaidam lithosphere, and other parameters.

4.3.3. Modeled Shape of the Basin Based on Two-Load Beam Flexural Modeling

Our estimate shows that when defining the width of the Qilian Shan and the Eastern Kunlun Shan to be 150 and 180 km, respectively, and the height of the Qilian Shan and the Eastern Kunlun Shan to be 2.5 and 1.2 km, respectively, the modeled deflection of the Qaidam basement provides the best fit to the original shape of the Qaidam basin obtained from shortening restoration and decompaction (Figures 7a and 7b). Different combinations of these parameters cannot improve the fit. In order to match with the restored shape of the basin during the deposition of Lulehe Fm., we systematically changed the height and width of the Qilian Shan load, while holding the height and width of Eastern Kunlun Shan load constant. On the other hand, we also changed the height and width of the Eastern Kunlun Shan load, while holding the height and width of Qilian Shan load constant in order to match with the restored shape of the basin during the deposition of Lulehe Fm. For instance, when increasing the width (e.g., 200 km) and decreasing the height (e.g., 2.0 km) of the Qilian Shan, the basement deflection is shallower (Figures 7c and 7d). When decreasing the width (e.g., 100 km) and increasing the height (e.g., 3.0 km) of the Qilian Shan, the basement deflection is too deep (Figures 7e and 7f). On the other hand, when increasing the width (e.g., 230 km) and decreasing the height (e.g., 0.8 km) of the Eastern Kunlun Shan, the basement deflection is shallower (Figures 7g and 7h), while decreasing the width (e.g., 130 km) and increasing the height (e.g., 1.7 km) of the Eastern Kunlun Shan results in a much deeper deflection curve (Figures 7i and 7j). Likewise, changing other parameters (e.g., flexural rigidity of the basement; Figure S9) also cannot improve the fit between the flexural loading models and estimates obtained from shortening restoration and decompaction.

We note that the original width of the basin changes depending on the applied Cenozoic shortening magnitude. For example, taking the 30% post-Lulehe shortening strain value of Yin, Dang, Zhang, et al. (2008) (Figure S8), the horizontal length of the original section DD' would be >330 km, much longer than the restored length using the estimate of shortening strain (~15%) by Wei et al. (2016) (Figure S7). However, even if we apply different shortening strains, the subsidence of the basin at point d would always exist, and the original shape of the basin after shortening restoration and decompaction could not be model by one-beam flexural modeling. We thus conclude that difference shortening strains would not change our inference of single Qilian Shan load fails to produce observed deflection of the Qaidam basement during the deposition of the Lulehe Fm.

In summary, the one-load beam flexural modeling reveals that the topographic load induced by the Qilian Shan alone cannot produce a sufficient load to cause the observed deflection of the Qaidam basement during the deposition of the Lulehe Fm. One the other hand, the two-load beam flexural estimate shows that under certain conditions (above-mentioned scale of the Qilian Shan and Eastern Kunlun Shan loads), the combined Eastern Kunlun Shan and the Qilian Shan topographic loads can jointly produce sufficient load to cause the observed deflection of the Qaidam basement during the deposition of the Lulehe Fm.

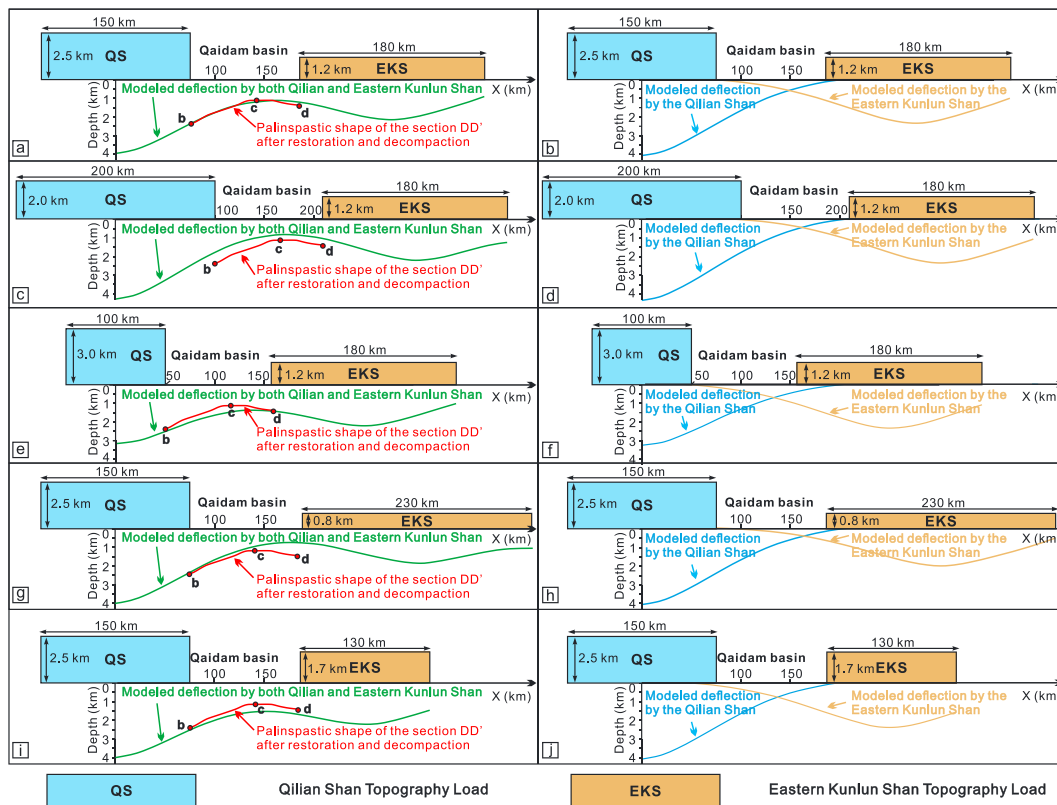


Figure 7. Two-load beam flexural modeling results, showing that both Qilian Shan and Eastern Kunlun Shan topographic loads can account for the flexural profile of Qaidam basement. We define the Qilian Shan and Eastern Kunlun Shan as rectangular blocks. (a), (c), (e), (g), and (i) show the total deflection from both the Qilian Shan and Eastern Kunlun Shan loads. (b), (d), (f), (h), and (j) show the individual deflection from Qilian Shan load and Eastern Kunlun Shan load, respectively. As shown in (a) and (b), when defining the width of the Qilian Shan and the Eastern Kunlun Shan to be 150 and 180 km, respectively, the height of Qilian Shan and Eastern Kunlun Shan to be 2.5 and 1.2 km, respectively, the modeled deflection of Qaidam basement fits the original shape of the Qaidam basin (section DD') obtained from shortening restoration and decompaction. Changing parameters, for example, (c) and (d) decreasing the height while increasing the width of Qilian Shan; (e) and (f) increasing the height while decreasing the width of Qilian Shan; (g) and (h) decreasing the height while increasing the width of Eastern Kunlun Shan; (i) and (j) increasing the height while decreasing the width of Eastern Kunlun Shan, cannot improve the fit between the modeled deflection of Qaidam basement and the original shape of the Qaidam basin (section DD') obtained from shortening restoration and decompaction.

5. Discussion

5.1. Paleogene Topography of the Qaidam Basin and Its Surroundings, Northern Tibet

Detailed sediment core description allows identification of the spatial distribution of lithofacies of the Lulehe Fm. We show that the Lulehe Fm. in the southwestern Qaidam basin, along the northern flank of the Eastern Kunlun Shan, mainly consists of distal fluvial to marginal lacustrine deposits together with limited proximal fluvial deposits. However, in both the northwestern (along the southern flank of the Altyn Tagh Shan) and northeastern Qaidam basin (along the southern flank of the Qilian Shan), the Lulehe Fm. is mainly characterized by a succession of coarse-grained proximal alluvial fan deposits (Figures S2, S4, and S6). The growth strata and associated strike slip and thrust faulting, shown in seismic profile AA' perpendicular to the Eastern Kunlun Shan, initiated during the early or middle Miocene, constraining the onset of deformation in the southwestern Qaidam basin and Eastern Kunlun Shan. However, faults rooted in the Altyn Tagh Shan and Qilian Shan, shown in seismic profiles BB' and CC' (Figure 3), initiated during the deposition of the Lulehe Fm., suggesting a simultaneous Paleogene onset of contraction within the Altyn Tagh Shan and Qilian Shan ranges. In addition, apatite fission track, (U-Th)/He, $^{40}\text{Ar}/^{39}\text{Ar}$ dating results (Clark et al., 2010; X. Chen et al., 2010; X. Chen et al., 2011; Duvall et al., 2013; Jolivet et al., 2001, 2003; Mock et al., 1999), as well as seismic profile interpretation (Cheng et al., 2014; Yin et al., 2007), reveal that the accelerated exhumation within the Eastern Kunlun Shan began in Oligocene to early Miocene time. Given that distal fluvial to marginal lacustrine deposits in the Lulehe Fm. developed in the southwestern

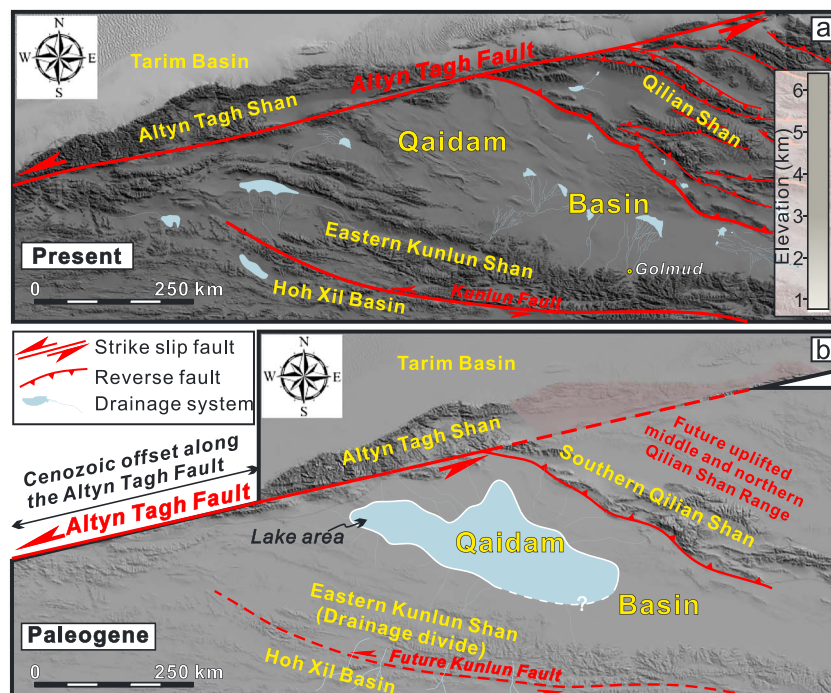


Figure 8. Proposed present-day and Paleogene topographic configuration of the Qaidam basin and its surroundings. The information the topography relief of the Qilian Shan is mainly based on the research by Bovet et al. (2009), Zhuang et al. (2011), and W. Wang et al. (2016), while the information on large-scale sinistral offset along the ATF and the topographic relief of Altyn Tagh Shan and Eastern Kunlun Shan are mainly based on the research by Cheng, Guo, et al. (2015); Cheng, Fu, et al. (2016); and Cheng, Jolivet, et al. (2016). Note that the topographic relief of the Eastern Kunlun Shan between the Qaidam basin and Hoh Xil basin during the Paleogene (deposition of the Lulehe Fm.). Considering the gradual lithofacies basinward transitions, from proximal alluvial fan to fluvial deposits along the margins of the basin to distal fluvial to marginal lacustrine deposits basinward, we infer a lake environment in the middle of the Qaidam basin during the deposition of the Lulehe Fm. The exact extent of the lake needs further investigation.

Qaidam basin, we thus propose, despite the fact that the Eastern Kunlun basement became the major source area for the southern Qaidam basin during the deposition of the Lulehe Fm., that the major topographic relief in the Eastern Kunlun Shan during the Paleogene was located further south than its present-day location. Structural and stratigraphic relationships in seismic lines adjacent to the Altyn Tagh Shan and Qilian Shan indicate that Paleogene deformation occurred near their present-day positions and resulted in the accumulation of proximal alluvial fan and thick conglomerate and sandstone along the northwestern and northeastern margins of the Qaidam basin (Figure 8). The analysis of sediment core samples generally displays gradual lithofacies basinward transitions, from proximal alluvial fan deposits along the margins of the basin to distal fluvial deposits basinward. By integrating the isopach map of the Lulehe Fm. with the subsurface data (including the core samples and the seismic profiles), we infer that the Qaidam basin is an internally drained Qaidam basin with relatively low topographic relief and received materials from the uplifted surrounding mountain belts during the deposition of Lulehe Fm. (Figures 3 and 8). This inference is also supported by the source to sink studies in this region (e.g., Bush et al., 2016; Cheng, Fu, et al., 2016).

The one-load beam flexural modeling results reveal that the single Qilian Shan topographic load is insufficient to account for the observed Paleogene sedimentary thickness and deflection of the Qaidam lithosphere. The subsidence of the basin at the point d (Figures 4 and 5) requires an additional topographic load along the southern margin of the Qaidam basin. The two-load beam flexural modeling results clearly show that when assuming both the Qilian Shan and the Eastern Kunlun Shan were exhumed and responsible for the deflection of the Qaidam basin, the modeled shape of the Qaidam basement can be matched with the original shape of the Qaidam basin (section DD') obtained from shortening restoration and decompaction. We thus infer that this additional load likely resulted from the exhumation of Eastern

Kunlun Shan during the deposition of the Lulehe Fm. The Eastern Kunlun Shan topographic load induced the subsidence along the southern margin of the basin, which is also evidenced by the sporadic subdecenter in the northern front of the Eastern Kunlun Shan during the deposition of the Lulehe Fm. (Figure 4b). We should note that the faulting in Fenghuoshan Thrust Belt to the south initiated during the Eocene-Oligocene (Staisch et al., 2014; Figure 1). However, given the present-day 400-km distance between the Fenghuoshan Thrust Belt and southern margin of the Qaidam basin, we infer that the contribution of the Fenghuoshan Thrust Belt topographic load is limited during the deposition of Lulehe Fm. Moreover, even if the Fenghuoshan Thrust Belt load account for some deflection of the Qaidam basin, the topographic loads from both Qilian Shan to the north and Fenghuoshan Thrust Belt to the south are insufficient to produce the subdecenter in the Qaidam basin, which is close to the Eastern Kunlun Shan (Figure 2).

In the context of the Paleo-Qaidam basin hypothesis, Yin, Dang, Zhang, et al. (2008) explained the minor southern Qaidam basin depocenter during the deposition of the Lulehe Fm. as have formed in localized synclines, which is comparable with the conclusion of classic buckling-type analog for northern Tibet (Burg et al., 1994). In this scenario, the deformation resulted from India-Asian collision was transferred northward to the Qilian Shan in the early Cenozoic, largely skipping the Qaidam basin, and some broad folds and widely spaced relatively minor faults existed across this region during the deposition of Lulehe Fm. However, based on the 3-D seismic profiles provided in this study (Figure 3) and previous work (Cheng et al., 2014), the onset time of deformation in the southern Qaidam basin is during the period when Shangganhaigou and Xiayoushashan formations deposited. In other words, the no (or extreme weak) deformation in the southern Qaidam basin challenges the likelihood of crustal bucking at that time.

Combing the widespread proximal fluvial deposits in the southern Qaidam basin with the flexural modeling results, we argue that the topographic loads generated by both the Eastern Kunlun Shan to the south and the Qilian Shan to the north are likely responsible for the subsidence of the Qaidam basin in the earliest part of the basin history (during the deposition of Lulehe Fm.). The flexural modeling results indicate that the Qaidam basin has been isolated since the deposition of the Lulehe Fm., forming an endorheic nonmarine basin. This inference of Eastern Kunlun topography during the deposition of Lulehe Fm. partly challenges the paleo-Qaidam model of Yin, Dang, Zhang, et al. (2008), which suggests that during the Paleogene (during the deposition of Lulehe, Lower Xiaganchaigou, Upper Xiaganchaigou, and Shangganhaigou formations), the Eastern Kunlun Shan had not exhumed and that the Qaidam and Hoh Xil basins formed single depression between the Qilian Shan to the north and the Fenghuo Shan thrust belt to the south. However, our two-load beam flexural modeling result shows a relative low topography in the Eastern Kunlun Shan during the deposition of Lulehe Fm. Integrating this low topography inference with some distal delta front deposits in the southern Qaidam basin, we infer that the Eastern Kunlun Shan topography was limited during the deposition of Lulehe Fm. and some of the topography was likely located further south than its present-day location. Although limited connection between the Qaidam basin with the potential source areas further south than the present-day location of the Eastern Kunlun Shan might exist, we speculate that the exhumed Eastern Kunlun Shan and Qilian Shan have created a topographic dam that impounded sediments supply since the deposition of the Lulehe Fm. Continuous accumulation of the clastic materials derived from Eastern Kunlun Shan and the Qilian Shan throughout the Cenozoic resulted in increased the sediment loading, which further contributes to the progressive subsidence of the closed Qaidam basin (e.g., Cheng et al., 2017, 2018; Métivier et al., 1998).

Despite uncertainties in the paleo-relief of the Qilian Shan and Eastern Kunlun Shan, the two-load beam flexural modeling suggests a relatively high (around 2.5 km) Qilian Shan comparing with the lower (around 1.0 km) Eastern Kunlun Shan. As indicated by the seismic profiles and sedimentary characteristics of Lulehe Fm. strata (Figures S1–S7), deformation along the northern margin of the Eastern Kunlun Shan was relatively minor, whereas the Qilian Shan was strongly deformed during the deposition of the Lulehe Fm. Although those frontal faults (e.g., Kunbei fault and Alaer fault) that root into the Eastern Kunlun Shan were inactive during the deposition of the Lulehe Fm., the presence of the Eastern Kunlun topographic load suggests that crustal deformation might have occurred further to the south, in the hinterland of the Eastern Kunlun Shan. We further propose that the intense deformation and relatively high relief of the southern Qilian Shan resulted in the accumulation of the proximal alluvial fan deposits along the northern Qaidam basin, while the weak deformation and low relief of the Eastern Kunlun Shan, located further south than

its present-day location, produced a mixture of proximal fluvial and distal fluvial to marginal lacustrine deposits along the southern margin of the Qaidam basin.

The best fit results based on the two-load beam flexural modeling also suggest that the modeled thickness of the Lulehe Fm. strata is slightly different from the original thickness estimates obtained from decompaction. (Figures 7a and 7b). Numerous newly acquired seismic profiles have revealed weak deformation within the Qaidam basin (especially in the interior of the basin) during the deposition of Lulehe Fm. that initiated since the deposition of the Shanggaichaigou-Xiaganchaigou Fm. (Figure 3; e.g., Cheng et al., 2014; Cheng, Fu, et al., 2016; Wei et al., 2016; Yin et al., 2007). We thus infer that the errors in thickness are partly related to an additional load resulting from the water load in the basin, the local Lulehe Fm. strata that were trapped into the Qaidam basin due to the growth of surrounding ranges during the deposition of the Lulehe Fm., and the potential preexisting topography of the Qaidam basement. (e.g., Bush et al., 2016; Cheng, Fu, et al., 2016; Li et al., 2017).

5.2. Paleogene Tectonic Deformation in the Northern Tibetan Plateau

Ascertaining whether the Paleogene deformation along the ATF is coupled with the crustal shortening in the Qilian Shan is important for understanding the kinematics of intraplate deformation associated with India-Asia collision and the dynamics of the Tibetan plateau growth. If the Paleogene deformation along the ATF was coupled with the crustal shortening in the Qilian Shan, we can infer that the large amount of sinistral displacement along the ATF since India-Asia collision was largely transferred into the Qilian Shan region, accommodated by oblique slip along faults in the mountain ranges; otherwise, such a large amount of deformation would be accommodated through left-lateral strike-slip displacement along the ATF and would be transferred to the region further to the east, beyond the Tibetan plateau (Cheng, Jolivet, et al., 2015; Cowgill et al., 2003; Darby et al., 2005; W. Wang et al., 2016; Yin et al., 2002; Yue et al., 2005; Yue et al., 2001; Zuza et al., 2016).

In our study, faults rooting into the Altyn Tagh Shan and Qilian Shan present on the seismic profile BB' and CC' (Figures 3b and 3c) are characterized by long-term activity since their Paleogene initiation, likely indicative of simultaneous deformation within both the Altyn Tagh Shan and the Qilian Shan since the Paleogene (since the deposition of the Lulehe Fm.). Therefore, the simultaneous deformation within the Altyn Tagh Shan and Qilian Shan since the Paleogene supports the idea that deformation in these two regions is kinematically linked. This finding also supports the idea that the initial faulting in the QSTB dates the onset of the ATF movement and the offset along the ATF since its initiation has been absorbed within the Qilian Shan (Cheng, Jolivet, et al., 2015; Cowgill et al., 2003; Yin et al., 2002; Yin, Dang, Wang, et al., 2008; Yin, Dang, Zhang, et al., 2008; Zuza et al., 2016). We further infer that the succession of synorogenic conglomerate deposited by a high-gradient depositional system (Zhuang et al., 2011) in the Lulehe Fm. records the initial growth of the northern Tibetan Plateau, which is in good agreement with some previous studies based on field investigation, seismic profile interpretation, and provenance analysis (Bush et al., 2016; Yin et al., 2007; Yin, Dang, Wang, et al., 2008; Yin, Dang, Zhang, et al., 2008; Zhuang et al., 2011).

Although the chronology of Lulehe Fm. is important for evaluating the intraplate response to the India-Asia collision and postcollisional convergence since circa 60–45 Ma (Garzanti and Van Haver, 1988; Green et al., 2008; Dupont-Nivet et al., 2010; Hu et al., 2015; W. Huang et al., 2015; Hu et al., 2016; Najman et al., 2010; Rowley, 1996), the depositional age of the Lulehe Fm. is highly debated. Based on magnetostratigraphy study, spore and pollen assemblages, regional lithostratigraphic correlation, and seismic reflection interpretation (Ji et al., 2017; Ke et al., 2013; Rieser et al., 2005, 2006; X. Wang et al., 2007; Xia et al., 2001; Yang et al., 1992; Zhang, 2006; Yin et al., 2007; Yin, Dang, Wang, et al., 2008; Yin, Dang, Zhang, et al., 2008), previous studies generally assigned a Paleocene to early Eocene basal age to the Lulehe Fm. However, recent magnetostratigraphy study of the Lulehe Fm. near the type locality in the northern Qaidam basin assigned an Oligocene (ca. 30 Ma) depositional age (W. Wang, Zheng, et al., 2017).

This large change in the basal age of Cenozoic strata in the Qaidam basin would result in a different kinematic evolution of the northern Tibetan plateau at 30 Ma with implications for crustal deformation mechanisms in the Tibetan plateau, (Burchfiel et al., 1991; Duvall & Clark, 2010; England & Houseman, 1986; Meyer et al., 1998; Ratschbacher et al., 1994; Yin, Dang, Wang, et al., 2008). Specifically, if considering a Paleocene to early Eocene depositional age (ca. 50 Ma) of the Lulehe Fm., the inception of the sinistral strike-slip

faulting along ATF and crustal shortening in the Qilian Shan should be around 50 Ma, which is as the same time as or shortly after the India-Asian collision. Given the 35-Ma initial exhumation of the Eastern Kunlun Shan (e.g., Clark et al., 2010; F. Wang, Shi, et al., 2017), some researchers have proposed that the strain derived from the India-Asia collision zone was transmitted rapidly at ~50 Ma to the northern and northeastern edge of the modern Tibetan plateau, followed by later pulses of plateau growth (Bush et al., 2016; Cheng, Guo, et al., 2015; Cheng, Jolivet, et al., 2016; Duvall et al., 2011; Jolivet et al., 2001; Yin et al., 2002, 2007; Yin, Dang, Wang, et al., 2008; Yin, Dang, Zhang, et al., 2008; Zhuang et al., 2011). On the other hand, when adopting the Oligocene (ca. 30 Ma) depositional age of the Lulehe Fm., the initial deformation within the Altyn Tagh Shan and the Qilian Shan at this time is similar to the initial exhumation of the Eastern Kunlun Shan and the initial deformation within Xining-Minhe-Longzhong basin complex, as well as Dangchang basin (Dupont-Nivet et al., 2004; Dupont-Nivet et al., 2008; Horton et al., 2004). This would support a gradually expansion of the plateau and the mountain building in the northeastern edge of the plateau that significantly postdated Indo-Asian collision by ~15 to 20 Myr (W. Wang, Zheng, et al., 2017). Therefore, further research should be conducted to provide robust constraints on basin-wide the depositional age of the Lulehe Fm.

6. Conclusions

Ascertaining the sedimentary and tectonic evolution of the Paleogene Lulehe Fm., which marks the onset of Cenozoic deposition in the Qaidam basin, helps to characterize the initial tectonics and topography of the northern Tibetan plateau.

Based on sediment core samples investigation, we show that the Lulehe Fm. mainly consists of distal fluvial to marginal lacustrine deposits together with additional proximal fluvial deposits along the northern front of the Eastern Kunlun Shan, whereas it is dominated by a succession of proximal alluvial fan deposits along the southern flank of the Altyn Tagh Shan and Qilian Shan. The Lulehe Fm. gradually displays basinward lithofacies transitions, from proximal alluvial fan to fluvial deposits along the margins of the basin to distal fluvial to marginal lacustrine deposits basinward.

Fault offset and growth structures shown on seismic profiles imply simultaneous contractional deformation in the Altyn Tagh Shan and Qilian Shan during the deposition of the Lulehe Fm. This inference of the simultaneous deformation supports the idea that deformation in Altyn Tagh Shan and the Qilian Shan has been kinematically linked since the Paleogene.

Furthermore, seismic profile interpretation, lithofacies evidence, and flexural loading estimates indicate that the Eastern Kunlun Shan was exhumed and shed detritus to the Qaidam basin during the deposition of the Lulehe Fm. The topographic loads generated by both the Eastern Kunlun Shan (with lower elevation) to the south and the Qilian Shan (with higher elevation) to the north are likely responsible for the flexural deflection of the Qaidam basement during the deposition of the Lulehe Fm. However, the relief of the Eastern Kunlun Shan was limited and was likely located further south than its present-day location. Collectively, we conclude that the Cenozoic initial subsidence of the Qaidam basin and the deflection of the Qaidam basement are driven by the topographic load of both the Qilian Shan to the north and the Eastern Kunlun Shan to the south. These results highlight the initial topography exhumation in the northern Tibetan plateau during the early Cenozoic.

References

- Allen, M. B., Walters, R. J., Song, S., Saville, C., De Paola, N., Ford, J., et al. (2017). Partitioning of oblique convergence coupled to the fault locking behavior of fold-and-thrust belts: Evidence from the Qilian Shan, northeastern Tibetan plateau. *Tectonics*, *36*, 1679–1698. <https://doi.org/10.1002/2017TC004476>
- Allen, P. A., & Allen, J. R. (2013). *Basin analysis: Principles and application to petroleum play assessment*. Oxford, UK: John Wiley & Sons.
- Bird, P. (1991). Lateral extrusion of lower crust from under high topography in the isostatic limit. *Journal of Geophysical Research*, *96*(B6), 10,275–10,286. <https://doi.org/10.1029/91JB00370>
- Bovet, P. M., Ritts, B. D., Gehrels, G., Abbink, A. O., Darby, B., & Hourigan, J. (2009). Evidence of Miocene crustal shortening in the north Qilian Shan from Cenozoic stratigraphy of the western Hexi Corridor, Gansu Province, China. *American Journal of Science*, *309*(4), 290–329. <https://doi.org/10.2475/00.4009.02>
- Braitenberg, C., Wang, Y., Fang, J., & Hsu, H. (2003). Spatial variations of flexure parameters over the Tibet-Qinghai plateau. *Earth and Planetary Science Letters*, *205*(3–4), 211–224. [https://doi.org/10.1016/S0012-821X\(02\)01042-7](https://doi.org/10.1016/S0012-821X(02)01042-7)
- Burchfiel, B. C., Quidong, D., Molnar, P., Royden, L., Yipeng, W., Peizhen, Z., & Weiqi, Z. (1989). Intracrustal detachment within zones of continental deformation. *Geology*, *17*(8), 748–752. [https://doi.org/10.1130/0091-7613\(1989\)017<0448:IDWZOC>2.3.CO;2](https://doi.org/10.1130/0091-7613(1989)017<0448:IDWZOC>2.3.CO;2)

Acknowledgments

The research was funded by grants from the National Science Foundation (EAR-1348005 and OISE-1545859) to Garzzone, National Science and Technology Major Project of China (Grant 2017ZX05008-001) to Guo, and Open project fund from State Key Laboratory of Loess and Quaternary Geology, Institute of Earth Environment, Chinese Academy of Sciences (SKLLQG1701) to Cheng. Permission of Qinghai Oilfield Company, PetroChina, for publication of reflection seismic data in Figure and isopach data in Figures and is acknowledged. SRTM digital topography is from <http://www.gscloud.cn>, and the original data for the decompaction analysis are available in the supporting information. We would like to thank Editor Nathan Niemi, reviewer Andrew Zuza, Devon Orme, and the other four anonymous reviewers for insightful suggestions that significantly improved the manuscript. We declare no competing financial interests.

- Burchfiel, B., Zhang, P., Wang, Y., Zhang, W., Song, F., Deng, Q., et al. (1991). Geology of the Haiyuan fault zone, Ningxia-Hui Autonomous Region, China, and its relation to the evolution of the northeastern margin of the Tibetan Plateau. *Tectonics*, *10*(6), 1091–1110. <https://doi.org/10.1029/90TC02685>
- Burg, J. P., Davy, P., & Martinod, J. (1994). Shortening of analogue models of the continental lithosphere: new hypothesis for the formation of the Tibetan plateau. *Tectonics*, *13*(2), 475–483. <https://doi.org/10.1029/93TC02738>
- Bush, M. A., Saylor, J. E., Horton, B. K., & Nie, J. (2016). Growth of the Qaidam Basin during Cenozoic exhumation in the northern Tibetan Plateau: Inferences from depositional patterns and multiproxy detrital provenance signatures. *Lithosphere*, *8*(1), 58–82. <https://doi.org/10.1130/L449.1>
- Cao, Z., Sun, X., Wang, L., Yan, C., Zhao, J., & Ma, F. (2013). The gas accumulation conditions of Dongping-Niudong slope area in front of Aerjin Mountain of Qaidam Basin (in Chinese with English abstract). *Natural Gas Geoscience*, *24*(6), 1125–1131.
- Chen, J.-L., Yin, A., Xu, J.-F., Dong, Y.-H., & Kang, Z.-Q. (2018). Late Cenozoic magmatic inflation, crustal thickening, and > 2 km of surface uplift in Central Tibet. *Geology*, *46*(1), 19–22. <https://doi.org/10.1130/G39699.1>
- Chen, X., Mcrivette, M., Li, L., Yin, A., Jiang, R., Wan, J., & Li, H. (2011). Thermochronological evidence for multi-phase uplifting of the East Kunlun Mountains, northern Tibetan Plateau (in Chinese with English abstract). *Geological Bulletin of China*, *30*(11), 1647–1660.
- Chen, X., Yuqi, D., An, Y., Liqun, W., Wuming, J., Rongbao, J., Suping, Z., et al. (2010). *Basin-mountain coupling and tectonic evolution of the Qaidam Basin and its adjacent orogenic belts* (in Chinese) (pp. 1–365). Beijing: Geological Publishing House.
- Chen, Y., Gilder, S., Halim, N., Cogné, J. P., & Courtillot, V. (2002). New paleomagnetic constraints on central Asian kinematics: Displacement along the Altyn Tagh fault and rotation of the Qaidam Basin. *Tectonics*, *21*(5), 1042. <https://doi.org/10.1029/2001TC901030>
- Chen, Z. L., Zhang, Y. Q., Wang, X. F., & Chen, X. H. (2001). Fission track dating of apatite constrains on the Cenozoic uplift of the Altyn Tagh Mountain (in Chinese with English abstract). *Acta Geoscientia Sinica*, *22*(5), 413–418.
- Cheng, F., Fu, S., Jolivet, M., Zhang, C., & Guo, Z. (2016). Source to sink relation between the eastern Kunlun range and the Qaidam Basin, northern Tibetan Plateau, during the Cenozoic. *Geological Society of America Bulletin*, *128*(1–2), 258–283.
- Cheng, F., Garzzone, C., Jolivet, M., Guo, Z., Zhang, D., & Zhang, C. (2018). A new sediment accumulation model of Cenozoic depositional ages from the Qaidam basin, Tibetan Plateau. *Journal of Geophysical Research: Earth Surface*, *123*, 3101–3121. <https://doi.org/10.1029/2018JF004645>
- Cheng, F., Garzzone, C., Jolivet, M., Wang, W., Dong, J., Richter, F., & Guo, Z. (2019). Provenance analysis of the Yumen Basin and northern Qilian Shan: Implications for the pre-collisional paleogeography in the NE Tibetan plateau and eastern termination of Altyn Tagh fault. *Gondwana Research*, *65*, 156–171. <https://doi.org/10.1016/j.jgr.2018.08.009>
- Cheng, F., Guo, Z., Jenkins, H. S., Fu, S., & Cheng, X. (2015). Initial rupture and displacement on the Altyn Tagh fault, northern Tibetan Plateau: Constraints based on residual Mesozoic to Cenozoic strata in the western Qaidam Basin. *Geosphere*, *11*(3), 921–942. <https://doi.org/10.1130/GES01070.1>
- Cheng, F., Jolivet, M., Dupont-Nivet, G., Wang, L., Yu, X., & Guo, Z. (2015). Lateral extrusion along the Altyn Tagh fault, Qilian Shan (NE Tibet): Insight from a 3D crustal budget. *Terra Nova*, *27*(6), 416–425. <https://doi.org/10.1111/ter.12173>
- Cheng, F., Jolivet, M., Fu, S., Zhang, C., Zhang, Q., & Guo, Z. (2016). Large-scale displacement along the Altyn Tagh Fault (North Tibet) since its Eocene initiation: Insight from detrital zircon U-Pb geochronology and subsurface data. *Tectonophysics*, *677–678*, 261–279.
- Cheng, F., Jolivet, M., Fu, S., Zhang, Q., Guan, S., Yu, X., & Guo, Z. (2014). Northward growth of the Qimen Tagh Range: A new model accounting for the Late Neogene strike-slip deformation of the SW Qaidam Basin. *Tectonophysics*, *632*, 32–47. <https://doi.org/10.1016/j.tecto.2014.05.034>
- Cheng, F., Jolivet, M., Hallot, E., Zhang, D., Zhang, C., & Guo, Z. (2017). Tectono-magmatic rejuvenation of the Qaidam craton, northern Tibet. *Gondwana Research*, *49*, 248–263. <https://doi.org/10.1016/j.jgr.2017.06.004>
- Clark, M. K. (2012). Continental collision slowing due to viscous mantle lithosphere rather than topography. *Nature*, *483*(7387), 74–77. <https://doi.org/10.1038/nature10848>
- Clark, M. K., Farley, K. A., Zheng, D., Wang, Z., & Duvall, A. R. (2010). Early Cenozoic faulting of the northern Tibetan Plateau margin from apatite (U-Th)/He ages. *Earth and Planetary Science Letters*, *296*(1–2), 78–88. <https://doi.org/10.1016/j.epsl.2010.04.051>
- Cowgill, E., Yin, A., Harrison, T. M., & Xiao-Feng, W. (2003). Reconstruction of the Altyn Tagh fault based on U-Pb geochronology: Role of back thrusts, mantle sutures, and heterogeneous crustal strength in forming the Tibetan Plateau. *Journal of Geophysical Research*, *108*(B7), 2346. <https://doi.org/10.1029/2002JB002080>
- Craddock, W. H., Kirby, E., Zhang, H., Clark, M. K., Champagnac, J.-D., & Yuan, D. (2014). Rates and style of Cenozoic deformation around the Gonghe Basin, northeastern Tibetan Plateau. *Geosphere*, *10*(6), 1255–1282. <https://doi.org/10.1130/GES01024.1>
- Darby, B. J., Ritts, B. D., Yue, Y., & Meng, Q. (2005). Did the Altyn Tagh fault extend beyond the Tibetan Plateau? *Earth and Planetary Science Letters*, *240*(2), 425–435. <https://doi.org/10.1016/j.epsl.2005.09.011>
- DeCelles, P. G. (2011). Foreland basin systems revisited: Variations in response to tectonic settings. In *Tectonics of sedimentary basins. Recent advances* (pp. 405–426). Oxford: Wiley-Blackwell.
- DeCelles, P. G., & Giles, K. A. (1996). Foreland basin systems. *Basin Research*, *8*(2), 105–123. <https://doi.org/10.1046/j.1365-2117.1996.01491.x>
- Delville, N., Arnaud, N., Montel, J.-M., Roger, F., Brunel, M., Tapponnier, P., & Sobel, E. (2001). Paleozoic to Cenozoic deformation along the Altyn Tagh fault in the Altun Shan massif area, eastern Qilian Shan, northeastern Tibet, China. *Geological Society of America Memoirs*, *194*, 269–292.
- Dewey, J. F., & Bird, J. M. (1970). Mountain belts and the new global tectonics. *Journal of Geophysical Research*, *75*(14), 2625–2647. <https://doi.org/10.1029/JB075i014p02625>
- Dupont-Nivet, G., Hoorn, C., & Komert, M. (2008). Tibetan uplift prior to the Eocene-Oligocene climate transition: Evidence from pollen analysis of the Xining Basin. *Geology*, *36*(12), 987–990. <https://doi.org/10.1130/G25063A.1>
- Dupont-Nivet, G., Horton, B., Butler, R., Wang, J., Zhou, J., & Waanders, G. (2004). Paleogene clockwise tectonic rotation of the Xining-Lanzhou region, northeastern Tibetan Plateau. *Journal of Geophysical Research*, *109*, B04401. <https://doi.org/10.1029/2003JB002620>
- Dupont-Nivet, G., Lippert, P. C., Van Hinsbergen, D. J. J., Meijers, M. J. M., & Kapp, P. (2010). Palaeolatitude and age of the Indo-Asia collision: Palaeomagnetic constraints. *Geophysical Journal International*, *182*(3), 1189–1198. <https://doi.org/10.1111/j.1365-246X.2010.04697.x>
- Duvall, A. R., & Clark, M. K. (2010). Dissipation of fast strike-slip faulting within and beyond northeastern Tibet. *Geology*, *38*(3), 223–226. <https://doi.org/10.1130/G30711.1>

- Duvall, A. R., Clark, M. K., Kirby, E., Farley, K. A., Craddock, W. H., Li, C., & Yuan, D.-Y. (2013). Low-temperature thermochronometry along the Kunlun and Haiyuan Faults, NE Tibetan Plateau: Evidence for kinematic change during late-stage orogenesis. *Tectonics*, 32, 1190–1211. <https://doi.org/10.1002/tect.20072>
- Duvall, A. R., Clark, M. K., van der Pluijm, B. A., & Li, C. (2011). Direct dating of Eocene reverse faulting in northeastern Tibet using Ar-dating of fault clays and low-temperature thermochronometry. *Earth and Planetary Science Letters*, 304(3–4), 520–526. <https://doi.org/10.1016/j.epsl.2011.02.028>
- England, P., & Houseman, G. (1986). Finite strain calculations of continental deformation: 2. Comparison with the India-Asia collision zone. *Journal of Geophysical Research*, 91(B3), 3664–3676.
- Fang, X., Zhang, W., Meng, Q., Gao, J., Wang, X., King, J., Song, C., et al. (2007). High-resolution magnetostratigraphy of the Neogene Huaitoutala section in the eastern Qaidam Basin on the NE Tibetan Plateau, Qinghai Province, China and its implication on tectonic uplift of the NE Tibetan Plateau. *Earth and Planetary Science Letters*, 258(1–2), 293–306. <https://doi.org/10.1016/j.epsl.2007.03.042>
- Fu, B., & Awata, Y. (2007). Displacement and timing of left-lateral faulting in the Kunlun Fault Zone, northern Tibet, inferred from geologic and geomorphic features. *Journal of Asian Earth Sciences*, 29(2–3), 253–265. <https://doi.org/10.1016/j.jseas.2006.03.004>
- Fu, L., Guan, P., Jian, X., Liu, R., Feng, F., An, Q., & Fan, C. (2012). Sedimentary genetic types of coarse fragment of Paleogene Lulehe Formation in Qaidam Basin and time limit of the Tibetan Plateau uplift (in Chinese with English abstract). *Natural Gas Geoscience*, 23(5), 833–840.
- Garzanti, E., & Van Haver, T. (1988). The indus clastics: Forearc basin sedimentation in the Ladakh Himalaya (India). *Sedimentary Geology*, 59(3–4), 237–249. [https://doi.org/10.1016/0037-0738\(88\)90078-4](https://doi.org/10.1016/0037-0738(88)90078-4)
- Gaudemer, Y., Tapponnier, P., Meyer, B., Peltzer, G., Shunmin, G., Zhitai, C., Huangung, D., et al. (1995). Partitioning of crustal slip between linked, active faults in the eastern Qilian Shan, and evidence for a major seismic gap, the 'Tianzhu gap', on the western Haiyuan Fault, Gansu (China). *Geophysical Journal International*, 120(3), 599–645. <https://doi.org/10.1111/j.1365-246X.1995.tb01842.x>
- Gehrels, G. E., Yin, A., & Wang, X. F. (2003). Detrital-zircon geochronology of the northeastern Tibetan plateau. *Geological Society of America Bulletin*, 115(7), 881–896. [https://doi.org/10.1130/0016-7606\(2003\)115<0881:DGOTNT>2.0.CO;2](https://doi.org/10.1130/0016-7606(2003)115<0881:DGOTNT>2.0.CO;2)
- Gong, S., Shou, J., Huang, P., Li, M., & Wang, Y. (2012). Sedimentary characteristic of braided delta in Lulehe Formation of Kunbei oilfield in Qaidam Basin (in Chinese with English abstract). *Chinese Journal of Geology*, 47(1), 116–128.
- Green, O. R., Searle, M. P., Corfield, R. I., & Corfield, R. M. (2008). Cretaceous-Tertiary carbonate platform evolution and the age of the India-Asia collision along the Ladakh Himalaya (Northwest India). *The Journal of Geology*, 116(4), 331–353. <https://doi.org/10.1086/588831>
- Horton, B., Dupont-Nivet, G., Zhou, J., Waanders, G., Butler, R., & Wang, J. (2004). Mesozoic-Cenozoic evolution of the Xining-Minhe and Dangchang basins, northeastern Tibetan Plateau: Magnetostratigraphic and biostratigraphic results. *Journal of Geophysical Research*, 109, B04402. <https://doi.org/10.1029/2003JB002913>
- Hu, X., Garzanti, E., Moore, T., & Raffi, I. (2015). Direct stratigraphic dating of India-Asia collision onset at the Selandian (middle Paleocene, 59±1 Ma). *Geology*, 43(10), 859–862. <https://doi.org/10.1130/G36872.1>
- Hu, X., Wang, J., BouDagher-Fadel, M., Garzanti, E., & An, W. (2016). New insights into the timing of the India-Asia collision from the Paleogene Quxia and Jialazi formations of the Xigaze forearc basin, South Tibet. *Gondwana Research*, 32, 76–92. <https://doi.org/10.1016/j.jgr.2015.02.007>
- Huang, J., Zhang, C., Wu, Y., Tan, J., & Li, B. (2013). Reservoir characteristics and controlling factors in lower Tertiary of Dongping area in the Qaidam Basin (in Chinese with English abstract). *Special Oil and Gas Reservoirs*, 20(6), 25–29.
- Huang, W., Hinsbergen, D. J., Lippert, P. C., Guo, Z., & Dupont-Nivet, G. (2015). Paleomagnetic tests of tectonic reconstructions of the India-Asia collision zone. *Geophysical Research Letters*, 42, 2642–2649. <https://doi.org/10.1002/2015GL063749>
- Huo, G. (1990). *Petroleum geology of China: Oil fields in Qianghai and Xizang* (in Chinese with English abstract). Beijing: Chinese Petroleum Industry Press.
- Ji, J., Zhang, K., Clift, P. D., Zhuang, G., Song, B., Ke, X., & Xu, Y. (2017). High-resolution magnetostratigraphic study of the Paleogene-Neogene strata in the Northern Qaidam Basin: Implications for the growth of the Northeastern Tibetan Plateau. *Gondwana Research*, 46, 141–155. <https://doi.org/10.1016/j.jgr.2017.02.015>
- Jiang, B., Li, F., Zheng, R., Liu, Q., & Liu, D. (2010). Sedimentary facies of Paleogene Lulehe Formation in western segment of northern margin of Qaidam Basin [in Chinese with English abstract]. *Lithologic Reservoirs*, 22(1), 49–52.
- Jolivet, M., Brunel, M., Seward, D., Xu, Z., Yang, J., Malavielle, J., Roger, F., et al. (2003). Neogene extension and volcanism in the Kunlun fault zone, northern Tibet: New constraints on the age of the Kunlun Fault. *Tectonics*, 22(5), 1052. <https://doi.org/10.1029/2002TC001428>
- Jolivet, M., Brunel, M., Seward, D., Xu, Z., Yang, J., Roger, F., Tapponnier, P., et al. (2001). Mesozoic and Cenozoic tectonics of the northern edge of the Tibetan plateau: Fission-track constraints. *Tectonophysics*, 343(1–2), 111–134. [https://doi.org/10.1016/S0040-1951\(01\)00196-2](https://doi.org/10.1016/S0040-1951(01)00196-2)
- Jolivet, M., Roger, F., Arnaud, N., Brunel, M., Tapponnier, P., & Seward, D. (1999). Histoire de l'exhumation de l'Altun Shan: indications sur l'âge de la subduction du bloc du Tarim sous le système de l'Altyin Tagh (Nord Tibet). *Comptes Rendus de l'Académie des Sciences - Series IIA - Earth and Planetary Science*, 329(10), 749–755.
- Jordan, T. E. (1981). Thrust loads and foreland basin evolution, Cretaceous, western United States. *AAPG Bulletin*, 65(12), 2506–2520.
- Ke, X., Ji, J., Zhang, K., Kou, X., Song, B., & Wang, C. (2013). Magnetostratigraphy and anisotropy of magnetic susceptibility of the Lulehe Formation in the northeastern Qaidam Basin. *Acta Geologica Sinica-English Edition*, 87(2), 576–587.
- Kidd, W. S. F., & Molnar, P. (1988). Quaternary and active faulting observed on the 1985 Academia Sinica-Royal Society Geotraverse of Tibet. *Philosophical Transactions of the Royal Society of London A: Mathematical, Physical and Engineering Sciences*, 327(1594), 337–363. <https://doi.org/10.1098/rsta.1988.0133>
- Kirby, E., Harkins, N., Wang, E., Shi, X., Fan, C., & Burbank, D. (2007). Slip rate gradients along the eastern Kunlun fault. *Tectonics*, 26, TC2010. <https://doi.org/10.1029/2006TC002033>
- Lease, R. O. (2014). Cenozoic mountain building on the northeastern Tibetan Plateau. *Geological Society of America Special Papers*, 507, 115–127. [https://doi.org/10.1130/2014.2507\(06\)](https://doi.org/10.1130/2014.2507(06))
- Lease, R. O., Burbank, D. W., Zhang, H., Liu, J., & Yuan, D. (2012). Cenozoic shortening budget for the northeastern edge of the Tibetan Plateau: Is lower crustal flow necessary? *Tectonics*, 31, TC3011. <https://doi.org/10.1029/2011TC003066>
- Li, L., Garzanti, C. N., Pullen, A., Zhang, P., & Li, Y. (2017). Late Cretaceous-Cenozoic basin evolution and topographic growth of the Hoh Xil Basin, central Tibetan Plateau. *GSA Bulletin*. <https://doi.org/10.1130/B31769.1>
- Lin, A., & Guo, J. (2008). Nonuniform slip rate and millennial recurrence interval of large earthquakes along the eastern segment of the Kunlun Fault, Northern Tibet. *Bulletin of the Seismological Society of America*, 98(6), 2866–2878. <https://doi.org/10.1785/0120070193>

- Lu, H., & Xiong, S. (2009). Magnetostratigraphy of the Dahonggou section, northern Qaidam Basin and its bearing on Cenozoic tectonic evolution of the Qilian Shan and Altyn Tagh Fault. *Earth and Planetary Science Letters*, 288(3-4), 539–550. <https://doi.org/10.1016/j.epsl.2009.10.016>
- Ma, D., & Wang, Y. (2015). New understandings and exploration discovery of Paleogene reservoirs of Kunbei fault terrace belt, Qaidam Basin, NW China (in Chinese with English abstract). *Petroleum Exploration and Development*, 42(4), 580–588. [https://doi.org/10.1016/S1876-3804\(15\)30053-7](https://doi.org/10.1016/S1876-3804(15)30053-7)
- Mao, L., Xiao, A., Wu, L., Li, B., Wang, L., Lou, Q., Dong, Y., et al. (2014). Cenozoic tectonic and sedimentary evolution of southern Qaidam Basin, NE Tibetan Plateau and its implication for the rejuvenation of Eastern Kunlun Mountains. *Science China Earth Sciences*, 57(11), 2726–2739. <https://doi.org/10.1007/s11430-014-4951-z>
- Meng, Q. R., & Fang, X. (2008). Cenozoic tectonic development of the Qaidam Basin in the northeastern Tibetan Plateau. *Geological Society of America Special Papers*, 444, 1–24.
- Meng, Q. R., Hu, J. M., & Yang, F. Z. (2001). Timing and magnitude of displacement on the Altyn Tagh fault: Constraints from stratigraphic correlation of adjoining Tarim and Qaidam basins, NW China. *Terra Nova*, 13(2), 86–91. <https://doi.org/10.1046/j.1365-3121.2001.00320.x>
- Métivier, F., Gaudemer, Y., Tapponnier, P., & Meyer, B. (1998). Northeastward growth of the Tibet plateau deduced from balanced reconstruction of two depositional areas: The Qaidam and Hexi Corridor basins, China. *Tectonics*, 17(6), 823–842. <https://doi.org/10.1029/98TC02764>
- Meyer, B., Tapponnier, P., Bourjot, L., Métiévier, F., Gaudemer, Y., Peltzer, G., Shunmin, G., et al. (1998). Crustal thickening in Gansu-Qinghai, lithospheric mantle subduction, and oblique, strike-slip controlled growth of the Tibet plateau. *Geophysical Journal International*, 135(1), 1–47. <https://doi.org/10.1046/j.1365-246X.1998.00567.x>
- Mo, F., Mou, Z., Chang, L., You, C., & Xu, L. (2013). Sedimentary facies of the lower Lulehe Formation in Qie 16 well block of Kunbei Oilfield (in Chinese with English abstract). *Lithologic Reservoirs*, 25(6), 14–19.
- Mock, C., Arnaud, N. O., & Cantagrel, J. M. (1999). An early unroofing in northeastern Tibet? Constraints from $^{40}\text{Ar}/^{39}\text{Ar}$ thermochronology on granitoids from the eastern Kunlun range (Qianghai, NW China). *Earth and Planetary Science Letters*, 171(1), 107–122. [https://doi.org/10.1016/S0012-821X\(99\)00133-8](https://doi.org/10.1016/S0012-821X(99)00133-8)
- Molnar, P., & Tapponnier, P. (1975). Cenozoic tectonics of Asia: Effects of a continental collision. *Science*, 189(4201), 419–426. <https://doi.org/10.1126/science.189.4201.419>
- Mu, J. (2002). The features of tertiary sequence stratigraphy and their controlling factors in the Hong-Shi area of Qaidam basin (in Chinese with English abstract), (PhD thesis, 163 pp.). China University of Geosciences.
- Najman, Y., Appel, E., Boudagher-Fadel, M., Bown, P., Carter, A., Garzanti, E., Godin, L., et al. (2010). Timing of India-Asia collision: Geological, biostratigraphic, and palaeomagnetic constraints. *Journal of Geophysical Research*, 115, B12416. <https://doi.org/10.1029/2010JB007673>
- Price, R. (1973). Large-scale gravitational flow of supracrustal rocks, southern Canadian Rockies. *Gravity and Tectonics*, 491–502.
- Qiu, N. S. (2002). Tectono-thermal evolution of the Qaidam Basin, China: Evidence from R_o and apatite fission track data. *Petroleum Geoscience*, 8(3), 279–285.
- Ratschbacher, L., Frisch, W., Liu, G., & Chen, C. (1994). Distributed deformation in southern and western Tibet during and after the India-Asia collision. *Journal of Geophysical Research*, 99(B10), 19,917–19,945.
- Rieser, A. B., Liu, Y., Genser, J., Neubauer, F., Handler, R., Friedl, G., & Ge, X. H. (2006). $^{40}\text{Ar}/^{39}\text{Ar}$ ages of detrital white mica constrain the Cenozoic development of the intracontinental Qaidam Basin, China. *GSA Bulletin*, 118(11-12), 1522–1534. <https://doi.org/10.1130/B25962.1>
- Rieser, A. B., Neubauer, F., Liu, Y., & Ge, X. (2005). Sandstone provenance of north-western sectors of the intracontinental Cenozoic Qaidam Basin, western China: Tectonic vs. climatic control. *Sedimentary Geology*, 177(1-2), 1–18. <https://doi.org/10.1016/j.sedgeo.2005.01.012>
- Ritts, B. D., & Biffi, U. (2000). Magnitude of post-Middle Jurassic (Bajocian) displacement on the central Altyn Tagh fault system, Northwest China. *Geological Society of America Bulletin*, 112(1), 61–74. [https://doi.org/10.1130/0016-7606\(2000\)112<61:MOPJBD>2.0.CO;2](https://doi.org/10.1130/0016-7606(2000)112<61:MOPJBD>2.0.CO;2)
- Ritts, B. D., Hanson, A. D., Zinniker, D., & Moldowan, J. M. (1999). Lower-Middle Jurassic nonmarine source rocks and petroleum systems of the northern Qaidam basin, Northwest China. *AAPG Bulletin*, 83(12), 1980–2005.
- Ritts, B. D., Yue, Y., & Graham, S. A. (2004). Oligocene-Miocene tectonics and sedimentation along the Altyn Tagh Fault, Northern Tibetan Plateau: Analysis of the Xorkol, Subei, and Aksay Basins. *The Journal of Geology*, 112(2), 207–229. <https://doi.org/10.1086/381658>
- Rowley, D. B. (1996). Age of initiation of collision between India and Asia: A review of stratigraphic data. *Earth and Planetary Science Letters*, 145(1–4), 1–13. [https://doi.org/10.1016/S0012-821X\(96\)00201-4](https://doi.org/10.1016/S0012-821X(96)00201-4)
- Royden, L., & Karner, G. D. (1984). Flexure of the continental lithosphere beneath Apennine and Carpathian foredeep basins. *Nature*, 309(5964), 142–144. <https://doi.org/10.1038/309142a0>
- Royden, L. H., Burchfiel, B. C., King, R. W., Wang, E., Chen, Z., Shen, F., & Liu, Y. (1997). Surface deformation and lower crustal flow in eastern Tibet. *Science*, 276(5313), 788–790. <https://doi.org/10.1126/science.276.5313.788>
- Saylor, J. E., Jordan, J. C., Sundell, K. E., Wang, X., Wang, S., & Deng, T. (2017). Topographic growth of the Jishi Shan and its impact on basin and hydrology evolution, NE Tibetan Plateau. *Basin Research*, 30(3), 544–563. <https://doi.org/10.1111/bre.12264>
- Sclater, J. G., & Christie, P. (1980). Continental stretching: an explanation of the post-Mid-Cretaceous subsidence of the central North Sea basin. *Journal of Geophysical Research*, 85(B7), 3711–3739. <https://doi.org/10.1029/JB085iB07p03711>
- Shi, D. N., Shen, Y., Zhao, W. J., & Li, A. B. (2009). Seismic evidence for a Moho offset and south-directed thrust at the easternmost Qaidam-Kunlun boundary in the Northeast Tibetan plateau. *Earth and Planetary Science Letters*, 288(1-2), 329–334. <https://doi.org/10.1016/j.epsl.2009.09.036>
- Sobel, E. R., Arnaud, N., Jolivet, M., Ritts, B. D., & Brunel, M. (2001). Jurassic to Cenozoic exhumation history of the Altyn Tagh range, Northwest China, constrained by $^{40}\text{Ar}/^{39}\text{Ar}$ and apatite fission track thermochronology. *Geological Society of America Memoirs*, 194, 247–267.
- Song, T., & Wang, X. (1993). Structural styles and stratigraphic patterns of syndepositional faults in a contractional setting: Examples from Qaidam basin, northwestern China. *AAPG Bulletin*, 77(1), 102–117.
- Staisch, L. M., Niemi, N. A., Hong, C., Clark, M. K., Rowley, D. B., & Currie, B. (2014). A Cretaceous-Eocene depositional age for the Fenghuoshan Group, Hoh Xil Basin: Implications for the tectonic evolution of the northern Tibet plateau. *Tectonics*, 33, 281–301. <https://doi.org/10.1002/2013TC003367>

- Sun, G. (2005). Sedimentary facies of the Tertiary in West Qaidam Basin (in Chinese with English abstract), (PhD thesis, 175 pp.). Chinese Academy of Sciences.
- Sun, G., Liu, W., Wang, B., Xu, L., Kang, J., & Wang, H. (2016). Reservoir characteristics of the Lulehe Formation in the Pingtai Area of the northern Qaidam basin (in Chinese with English abstract). *Acta Sedimentologica Sinica*, *34*(2), 356–363.
- Sun, Z. M., Yang, Z. Y., Pei, J. L., Ge, X. H., Wang, X. S., Yang, T. S., Li, W. M., et al. (2005). Magnetostratigraphy of Paleogene sediments from northern Qaidam Basin, China: Implications for tectonic uplift and block rotation in northern Tibetan plateau. *Earth and Planetary Science Letters*, *237*(3–4), 635–646. <https://doi.org/10.1016/j.epsl.2005.07.007>
- Tapponnier, P., Peltzer, G., & Armijo, R. (1986). On the mechanics of the collision between India and Asia. *Geological Society, London, Special Publications*, *19*(1), 113–157. <https://doi.org/10.1144/GSL.SP.1986.019.01.07>
- Tapponnier, P., Xu, Z. Q., Roger, F., Meyer, B., Arnaud, N., Wittlinger, G., & Yang, J. S. (2001). Oblique stepwise rise and growth of the Tibet Plateau. *Science*, *294*(5547), 1671–1677. <https://doi.org/10.1126/science.105978>
- Turcotte, D., & Schubert, G. (2002). *Geodynamics* (456 pp.). Cambridge, UK: Cambridge University Press.
- Van Der Woerd, J., Tapponnier, P., Ryerson, F. J., Meriaux, A. S., Meyer, B., Gaudemer, Y., Finkel, R. C., et al. (2002). Uniform postglacial slip-rate along the central 600 km of the Kunlun Fault (Tibet), from ²⁶Al, ¹⁰Be, and ¹⁴C dating of riser offsets, and climatic origin of the regional morphology. *Geophysical Journal International*, *148*(3), 356–388. <https://doi.org/10.1046/j.1365-246x.2002.01556.x>
- Van Hinsbergen, D. J., Lippert, P. C., Dupont-Nivet, G., McQuarrie, N., Doubrovine, P. V., Spakman, W., & Torsvik, T. H. (2012). Greater India Basin hypothesis and a two-stage Cenozoic collision between India and Asia. *Proceedings of the National Academy of Sciences*, *109*(20), 7659–7664. <https://doi.org/10.1073/pnas.1117262109>
- Wan, J. L., Wang, Y., Li, Q., Wang, F., & Wang, E. (2001). FT evidence of northern Altyn uplift in Late-Cenozoic (in Chinese with English abstract), bulletin of mineralogy, *Petrology and Geochemistry*, *20*(4), 222–224.
- Wang, C., Zhao, X., Liu, Z., Lippert, P. C., Graham, S. A., Coe, R. S., Yi, H., et al. (2008). Constraints on the early uplift history of the Tibetan Plateau. *Proceedings of the National Academy of Sciences*, *105*(13), 4987–4992. <https://doi.org/10.1073/pnas.0703595105>
- Wang, C. S., Gao, R., Yin, A., Wang, H., Zhang, Y. X., Guo, T. L., Li, Q. S., et al. (2011). A mid-crustal strain-transfer model for continental deformation: A new perspective from high-resolution deep seismic-reflection profiling across NE Tibet. *Earth and Planetary Science Letters*, *306*(3–4), 279–288. <https://doi.org/10.1016/j.epsl.2011.04.010>
- Wang, E. (1997). Displacement and timing along the northern strand of the Altyn Tagh fault zone, northern Tibet. *Earth and Planetary Science Letters*, *150*(1–2), 55–64. [https://doi.org/10.1016/S0012-821X\(97\)00085-X](https://doi.org/10.1016/S0012-821X(97)00085-X)
- Wang, E., Xu, F.-Y., Zhou, J.-X., Wan, J., & Burchfiel, B. C. (2006). Eastward migration of the Qaidam basin and its implications for Cenozoic evolution of the Altyn Tagh fault and associated river systems. *Geological Society of America Bulletin*, *118*(3–4), 349–365. <https://doi.org/10.1130/B25778.1>
- Wang, F., Lob, C.-H., Li, Q., Yeh, M.-W., Wan, J., Zheng, D., & Wang, E. (2004). Onset timing of significant unroofing around Qaidam basin, northern Tibet, China: Constraints from ⁴⁰Ar/³⁹Ar and FT thermochronology on granitoids. *Journal of Asian Earth Sciences*, *24*(1), 59–69. <https://doi.org/10.1016/j.jseas.2003.07.004>
- Wang, F., Shi, W., Zhang, W., Wu, L., Yang, L., Wang, Y., & Zhu, R. (2017). Differential growth of the northern Tibetan margin: Evidence for oblique stepwise rise of the Tibetan plateau. *Scientific Reports*, *7*(1), 41164. <https://doi.org/10.1038/srep41164>
- Wang, H., Tan, M., & Zhang, Y. (2014). Paleogeographic characteristics and evolution in Lulehe Formation, Qaidam Basin (in Chinese with English abstract). *Coal Geology of China*, *26*(10), 7–21.
- Wang, J., Zhang, C., Wu, Y., Tan, J., & Li, B. (2013). Reservoir characteristics and controlling factors of the early Cenozoic strata in the Dongping Area, NW Qaidam basin (in Chinese). *Special Oil & Gas Reservoirs*, *20*(6), 25–29.
- Wang, L., Xiao, A. C., Gong, Q. L., Liu, D., Wu, L., Zhou, S. P., Shen, Z. Y., et al. (2010). The unconformity in Miocene sequence of western Qaidam Basin and its tectonic significance. *Science China Earth Sciences*, *53*(8), 1126–1133. <https://doi.org/10.1007/s11430-010-4006-z>
- Wang, W., Zhang, P., Pang, J., Garzzone, C., Zhang, H., Liu, C., Zheng, D., et al. (2016). The Cenozoic growth of the Qilian Shan in the northeastern Tibetan Plateau: A sedimentary archive from the Jiuxi Basin. *Journal of Geophysical Research: Solid Earth*, *121*, 2235–2257. <https://doi.org/10.1002/2015JB012689>
- Wang, W., Zheng, W., Zhang, P., Li, Q., Kirby, E., Yuan, D., Zheng, D., et al. (2017). Expansion of the Tibetan Plateau during the Neogene. *Nature Communications*, *8*, 15887. <https://doi.org/10.1038/ncomms15887>
- Wang, X., Qiu, Z., Li, Q., Wang, B., Qiu, Z., Downs, W. R., Xie, G., et al. (2007). Vertebrate paleontology, biostratigraphy, geochronology, and paleoenvironment of Qaidam Basin in northern Tibetan Plateau. *Palaogeography, Palaeoclimatology, Palaeoecology*, *254*(3–4), 363–385. <https://doi.org/10.1016/j.palaeo.2007.06.007>
- Wang, Y., Nie, J., Zhang, T., Sun, G., Yang, X., Liu, Y., & Liu, X. (2010). Cenozoic tectonic evolution in the western Qaidam Basin inferred from subsurface data. *Geosciences Journal*, *14*(4), 335–344. <https://doi.org/10.1007/s12303-010-0033-1>
- Wang, Y., Zhang, X., Wang, E., Zhang, J., Li, Q., & Sun, G. (2005). ⁴⁰Ar/³⁹Ar thermochronological evidence for formation and Mesozoic evolution of the northern-central segment of the Altyn Tagh fault system in the northern Tibetan plateau. *Geological Society of America Bulletin*, *117*(9), 1336–1346. <https://doi.org/10.1130/B25685.1>
- Wangen, M. (2010). *Physical principles of sedimentary basin analysis*. Cambridge, UK: Cambridge University Press. <https://doi.org/10.1017/CBO9780511711824>
- Watts, A., Bodine, J., & Steckler, M. (1980). Observations of flexure and the state of stress in the oceanic lithosphere. *Journal of Geophysical Research*, *85*(B11), 6369–6376. <https://doi.org/10.1029/JB085iB11p06369>
- Wei, Y., Xiao, A., Wu, L., Mao, L., Zhao, H., Shen, Y., & Wang, L. (2016). Temporal and spatial patterns of Cenozoic deformation across the Qaidam Basin, Northern Tibetan Plateau. *Terra Nova*, *28*(6), 409–418. <https://doi.org/10.1111/ter.12234>
- Wu, L., Xiao, A., Ma, D., Li, H., Xu, B., Shen, Y., & Mao, L. (2014). Cenozoic fault systems in southwest Qaidam Basin, northeastern Tibetan Plateau: Geometry, temporal development, and significance for hydrocarbon accumulation. *AAPG Bulletin*, *98*(6), 1213–1234. <https://doi.org/10.1306/11131313087>
- Wu, L., Xiao, A., Wang, L., Shen, Z., Zhou, S., Chen, Y., Wang, L., et al. (2011). Late Jurassic-Early Cretaceous Northern Qaidam Basin, NW China: Implications for the earliest Cretaceous intracontinental tectonism. *Cretaceous Research*, *32*(4), 552–564. <https://doi.org/10.1016/j.cretres.2011.04.002>
- Wu, L., Xiao, A. C., Yang, S. F., Wang, L. Q., Mao, L. G., Wang, L., Dong, Y. P., et al. (2012). Two-stage evolution of the Altyn Tagh Fault during the Cenozoic: New insight from provenance analysis of a geological section in NW Qaidam Basin, NW China. *Terra Nova*, *24*(5), 387–395. <https://doi.org/10.1111/j.1365-3121.2012.01077.x>
- Xia, W. C., Zhang, N., Yuan, X. P., Fan, L. S., & Zhang, B. S. (2001). Cenozoic Qaidam basin, China: A stronger tectonic inverted, extensional rifted basin. *AAPG Bulletin*, *85*(4), 715–736.

- Xiao, Q., Shao, G., Liu-Zeng, J., Oskin, M. E., Zhang, J., Zhao, G., & Wang, J. (2015). Eastern termination of the Altyn Tagh Fault, western China: Constraints from a magnetotelluric survey. *Journal of Geophysical Research: Solid Earth*, *120*, 2838–2858. <https://doi.org/10.1002/2014JB011363>
- Yang, F., Ma, Z. Q., Xu, T. C., & Ye, S. J. (1992). A Tertiary paleomagnetic stratigraphic profile in Qaidam basin (in Chinese with English abstract). *Acta Petrologica Sinica*, *13*(2), 97–101.
- Yang, F., Zou, N., Shi, J., Long, G., Jiang, H., Liu, S., Du, Z., et al. (2013). Probability cumulative grain size curves in the Paleogene clastic sediments and Environmental significance in Maxian region of northern Qaidam Basin (in Chinese with English abstract). *Natural Gas Geoscience*, *24*(4), 690–700.
- Yi, H. S., Wang, C. S., Shi, Z. Q., Lin, J. H., & Zhu, L. D. (2008). Early uplift history of the Tibetan plateau: Records from paleocurrents and paleodrainage in the Hoh Xil basin. *Acta Geologica Sinica-English Edition*, *82*(1), 206–213.
- Yin, A., Dang, Y. Q., Wang, L. C., Jiang, W. M., Zhou, S. P., Chen, X. H., Gehrels, G. E., et al. (2008). Cenozoic tectonic evolution of Qaidam basin and its surrounding regions (part 1): The southern Qilian Shan-Nan Shan thrust belt and northern Qaidam basin. *Geological Society of America Bulletin*, *120*(7–8), 813–846. <https://doi.org/10.1130/B26180.1>
- Yin, A., Dang, Y. Q., Zhang, M., Chen, X. H., & McRivette, M. W. (2008). Cenozoic tectonic evolution of the Qaidam basin and its surrounding regions (part 3): Structural geology, sedimentation, and regional tectonic reconstruction. *Geological Society of America Bulletin*, *120*(7–8), 847–876. <https://doi.org/10.1130/B26232.1>
- Yin, A., Dang, Y. Q., Zhang, M., McRivette, M. W., Burgess, W. P., & Chen, X. H. (2007). Cenozoic tectonic evolution of Qaidam basin and its surrounding regions (part 2): Wedge tectonics in southern Qaidam basin and the Eastern Kunlun Range. *Geological Society of America Special Papers*, *433*, 369–390.
- Yin, A., & Harrison, T. M. (2000). Geologic evolution of the Himalayan-Tibetan orogen. *Annual Review of Earth and Planetary Sciences*, *28*(1), 211–280. <https://doi.org/10.1146/annurev.earth.28.1.211>
- Yin, A., Rumelhart, P., Butler, R., Cowgill, E., Harrison, T., Foster, D., Ingersoll, R., et al. (2002). Tectonic history of the Altyn Tagh fault system in northern Tibet inferred from Cenozoic sedimentation. *Geological Society of America Bulletin*, *114*(10), 1257–1295. [https://doi.org/10.1130/0016-7606\(2002\)114<1257:THOTAT>2.0.CO;2](https://doi.org/10.1130/0016-7606(2002)114<1257:THOTAT>2.0.CO;2)
- Yuan, D. Y., Ge, W. P., Chen, Z. W., Li, C. Y., Wang, Z. C., Zhang, H. P., Zhang, P. Z., et al. (2013). The growth of northeastern Tibet and its relevance to large-scale continental geodynamics: A review of recent studies. *Tectonics*, *32*, 1358–1370. <https://doi.org/10.1002/tect.20081>
- Yuan, W. M., Dong, J. Q., Wang, S. C., & Carter, A. (2006). Apatite fission track evidence for Neogene uplift in the eastern Kunlun Mountains, northern Qinghai-Tibet Plateau, China. *Journal of Asian Earth Sciences*, *27*(6), 847–856. <https://doi.org/10.1016/j.jseas.2005.09.002>
- Yue, Y. J., Graham, S. A., Ritts, B. D., & Wooden, J. L. (2005). Detrital zircon provenance evidence for large-scale extrusion along the Altyn Tagh fault. *Tectonophysics*, *406*(3–4), 165–178. <https://doi.org/10.1016/j.tecto.2005.05.023>
- Yue, Y. J., & Liou, J. G. (1999). Two-stage evolution model for the Altyn Tagh fault, China. *Geology*, *27*(3), 227–230. [https://doi.org/10.1130/0091-7613\(1999\)027<0227:TSEMFT>2.3.CO;2](https://doi.org/10.1130/0091-7613(1999)027<0227:TSEMFT>2.3.CO;2)
- Yue, Y. J., Ritts, B. D., & Graham, S. A. (2001). Initiation and long-term slip history of the Altyn Tagh Fault. *International Geology Review*, *43*(12), 1087–1093. <https://doi.org/10.1080/00206810109465062>
- Zhang, C., Cheng, F., Huang, G., Huang, Y., Xing, C., Guan, B., Zhang, Q., et al. (2013). Sediment and reservoir characteristics with reservoir evaluation of Lulehe Formation in Qie 16 block of Kunbei oilfield in Qaidam basin (in Chinese with English abstract). *Acta Petrologica Sinica*, *29*(8), 2883–2894.
- Zhang, H. P., Craddock, W. H., Lease, R. O., Wang, W. T., Yuan, D. Y., Zhang, P. Z., Molnar, P., et al. (2012). Magnetostratigraphy of the Neogene Chaka basin and its implications for mountain building processes in the north-eastern Tibetan Plateau. *Basin Research*, *24*(1), 31–50. <https://doi.org/10.1111/j.1365-2117.2011.00512.x>
- Zhang, W. (2006). The high precise Cenozoic magnetostratigraphy of the Qaidam Basin and uplift of the Northern Tibetan Plateau (in Chinese with English abstract), (PhD thesis, pp. 1–105). Lanzhou University, Lanzhou.
- Zheng, D., Clark, M. K., Zhang, P., Zheng, W., & Farley, K. A. (2010). Erosion, fault initiation and topographic growth of the North Qilian Shan (northern Tibetan Plateau). *Geosphere*, *6*(6), 937–941. <https://doi.org/10.1130/GES00523.1>
- Zhou, J. X., Xu, F. Y., Wang, T. C., Cao, A. F., & Yin, C. M. (2006). Cenozoic deformation history of the Qaidam Basin, NW China: Results from cross-section restoration and implications for Qinghai-Tibet Plateau tectonics. *Earth and Planetary Science Letters*, *243*(1–2), 195–210. <https://doi.org/10.1016/j.epsl.2005.11.033>
- Zhuang, G., Hourigan, J. K., Ritts, B. D., & Kent-Corson, M. L. (2011). Cenozoic multiple-phase tectonic evolution of the northern Tibetan Plateau: Constraints from sedimentary records from Qaidam basin, Hexi Corridor, and Subei Basin, northwest China. *American Journal of Science*, *311*(2), 116–152. <https://doi.org/10.2475/02.2011.02>
- Zuza, A. V., Cheng, X., & Yin, A. (2016). Testing models of Tibetan Plateau formation with Cenozoic shortening estimates across the Qilian Shan-Nan Shan thrust belt. *Geosphere*, *12*(2), 501–532. <https://doi.org/10.1130/GES01254.1>
- Zuza, A. V., Wu, C., Reith, R. C., Yin, A., Li, J., Zhang, J., Zhang, Y., et al. (2017). Tectonic evolution of the Qilian Shan: An early Paleozoic orogen reactivated in the Cenozoic. *GSA Bulletin*, *130*(5–6), 881–925. <https://doi.org/10.1130/B31721.1>
- Zuza, A. V., & Yin, A. (2016). Continental deformation accommodated by non-rigid passive bookshelf faulting: An example from the Cenozoic tectonic development of northern Tibet. *Tectonophysics*, *677*, 227–240.